ANALYTICAL SOLUTIONS FOR MULTIPLE-MATRIX IN FRACTURED RESERVOIRS:

APPLICATION TO CONVENTIONAL AND UNCONVENTIONAL RESERVOIRS

by

Mehmet Ali Torcuk

A thesis submitted to the Faculty and the Board of Trustees of the Colorado School of Mines in partial fulfillment of the requirements for the degree of Master of Science (Petroleum Engineering).

Golden, Colorado

Date _____

Signed: _____

Mehmet Ali Torcuk

Signed: _____

Dr. Hossein Kazemi

Thesis Advisor

Golden, Colorado

Date _____

Signed:_____

Dr. William Fleckenstein

Professor and Head

Department of Petroleum Engineering

ABSTRACT

In this thesis, I present a new method to model heterogeneity and flow channeling in petroleum reservoirs—specially reservoirs containing interconnected microfractures. The method is applicable both to conventional and unconventional reservoirs where the interconnected microfractures form the major flow path. The flow equations, which could include flow contributions from matrix blocks of various size, permeability and porosities, are solved by the Laplace transform analytical solutions and finite-difference numerical solutions. The accuracy of flow from and into nano-Darcy matrix blocks is of great interest to those dealing with unconventional reservoirs. Thus, matrix flow equations are solved using both pseudo-steady-state (PSS) and unsteady-state (USS) formulations.

The matrix blocks can be of different size and properties within the representative elementary volume (REV) in the analytical solutions and within each control volume (CV) in the numerical solutions. While the analytical solutions were developed for slightly compressible linear systems, the numerical solutions are general and can be used for non-linear multi-phase, multi-component flow problems.

The mathematical solutions were used to analyze the long-term performance of a gas well and two oil wells in two separate unconventional reservoirs. Finally, the formulations were used to assess enhanced oil recovery potential from a typical nano-Darcy matrix block. It is concluded that matrix contribution to flow is very slow in a typical low-permeability unconventional reservoir and much of the enhanced production is from the fluids contained in the microfractures than in the matrix.

In addition to field applications, the mathematical formulations and solution methods are presented in a transparent fashion to allow easy utilization of the techniques for reservoir and engineering applications.

TABLE OF CONTENTS

LIST OF FIGURES

LIST OF TABLES

ACKNOWLEDGEMENT

Firstly, I would like to thank my advisor, Dr. Hossein Kazemi, not only his contributions to this study but for the outstanding mentorship and guidance that he has provided me. His ideas opened up my horizon. I am thankful to members of dissertation committee: Dr. Azra Tutuncu, Dr. Yu-Shu Wu, and Dr. B. Todd Hoffman for their valuable comments on this study. I am also thankful to all professors in Petroleum Engineering Department at Colorado School of Mines, for their contributions to my academic background. Special thanks to Basak Kurtoglu for the valuable discussions, suggestions and comments she has provided me throughout the course of this thesis.

Financial assistance provided by Marathon Center of Excellence for Reservoir Studies (MCERS) is gratefully acknowledged.

During the course of this thesis, I have benefited from the kind assistance of many friends. First, I wish to express my sincere thanks to Denise Winn-Bower for her patience and helps. I am especially grateful to all my friends who are either in Turkey or in US. It is impossible to list all of your names here. I would like to thank them all for their enjoyable friendship.

Finally, but most deeply, I thank to my family and my girlfriend, Canan Aslan for the moral support that they have provided me.

This thesis is dedicated to my grandfather, Mehmet Ali Torcuk who had been a great source of inspiration.

CHAPTER 1
INTRODUCTION

Fractures in a petroleum reservoir are created by natural forces, by man-made interventions, or combination of the two. The natural fractures are created by folding, faulting, and subsidence of geologic structures over a long period of time. The giant carbonate oilfields in the Middle East are good examples of naturally fractured reservoirs. **Fig. 1.1** shows an outcrop of a fractured basement rock from Alcova reservoir in Wyoming overlain by Madison formation.

Figure 1.1: An outcrop of fractured basement rock from Alcova Reservoir, Wyoming (Courtesy: H. Kazemi, CSM)

In addition to the natural fractures, engineering activities, such as water injection and hydraulic fracture stimulation also cause creation of fractures in a petroleum reservoir. In the last decade, there has been a great interest in enhanced oil and gas recovery in unconventional shale reservoirs. To make shale reservoirs productive, multistage hydraulic fracturing has been used to break the tight shale matrix into smaller pieces to create larger surface areas of contact (microfractures). Multistage hydraulic fracturing creates a dual-porosity environment in the vicinity of the hydraulic fracture. An idealized schematic of a multi-stage hydraulic fracturing in an unconventional reservoir is shown in **Fig. 1.2**. The near wellbore region includes a high density of microfractures which are created by stress changes resulting from hydraulic fracture stimulation.

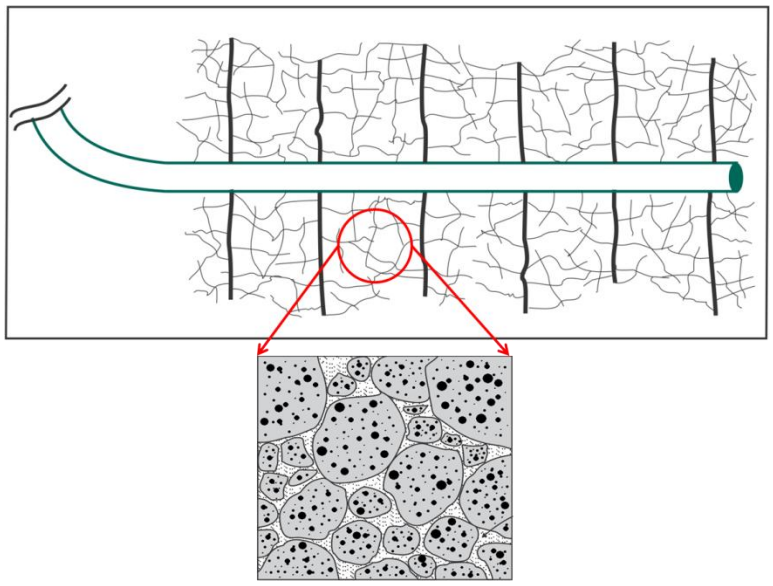

Figure 1.2: An idealized schematic of multi-stage hydraulic fracturing in unconventional reservoirs

Presence of fractures in petroleum reservoirs requires techniques to characterize flow in fractured reservoirs. Because of fractures' extreme heterogeneity and anisotropy, characterization of fractured reservoirs has been a challenging issue. For instance, fractures can negatively affect the success of an EOR project because of flow channeling of the injected fluids. On the other hand, primary production from unconventional reservoirs is enhanced because of the presence of fractures. Both in naturally fractured reservoirs and hydraulically fractured reservoirs, the matrix blocks are heterogeneous and have different sizes and shapes. To model fluid flow in a such fractured reservoir, the mathematical formulations must account for heterogeneity of the matrix blocks.

Mathematical models describing the fluid flow in dual-porosity media began with papers from Barenblatt et al. (1960) and Warren-Root (1963). These models assume pseudo-steady state (PSS) fluid transfer from matrix to fracture. Later, a model, which considered unsteady-state (USS) or transient fluid transfer between matrix and fracture, was reported by Kazemi (1969) and de Swaan-O (1976). The Barenblatt and Warren-Root models ignore spatial distribution of pressure and transient flow in the matrix block. Each matrix block is assigned an average pressure; that is it is assumed that pressure is uniform in the matrix block.

In this work, I focus on the modeling of fluid flow in naturally fractured conventional and unconventional reservoirs. A multiple-matrix model is presented to account for the flow contributions of various matrix blocks having different geometric shapes and different properties. The most common flow hierarchy in a fractured petroleum reservoir is: ***matrix*** to ***fracture*** to ***wellbore*** (if it is a naturally fractured

reservoir) or ***matrix*** to ***natural fractures*** to ***hydraulic fracture*** to ***wellbore*** (if it is a hydraulically fractured reservoir). In this study, I consider the 1D flow from matrix to natural fractures to a hydraulic fracture which is also the wellbore. I mainly focus on the developments of analytical solutions for multiple-matrix model. However, the multiple-matrix model presented in this study can be used for 3D numerical modeling of single and multi-phase flow. Furthermore, it can also be used in compositional modeling of petroleum reservoirs to capture PVT phase behavior variability in the matrix blocks.

The organization of this thesis is as follows: First, I give the formulation for single phase flow in a dual-porosity reservoir supported by a uniform set of matrix blocks (single-matrix case). Then this formulation is extended to multiple-matrix model where a non-uniform set of matrix blocks support flow into the fractures. Next, I present the relevant pseudo-steady state and unsteady state transfer functions. Then, I develop the Laplace domain analytical solutions for both the single- and multiple-matrix models. In addition, I provide the closed form solutions for pressure transient test applications. The theoretical development is followed by examples to show applications to field problems. In these field problems, I show the effects of heterogeneity variation of matrix blocks on well performance. Finally, I present a discussion on the work done and give the conclusion of the work.

CHAPTER 2

SINGLE-MATRIX AND MULTIPLE-MATRIX MODELS

The concept of dual-porosity modeling includes a continuum of interconnected fractures and a set of matrix blocks (cubes, spheres and slabs) imbedded in the fractures. However, in nature, the matrix block size and properties vary; which is the focus of this thesis. In this chapter, I first give the diffusivity equation for 1D fluid flow in dual-porosity reservoirs. Next, I present the basic definitions and equations used in the multiple-matrix model.

2.1 Homogeneous Single-Matrix Model

Naturally fractured dual-porosity reservoirs are usually idealized as a set of uniform matrix blocks with the geometric shapes of cube, sphere and slab (**Fig. 2.1**).

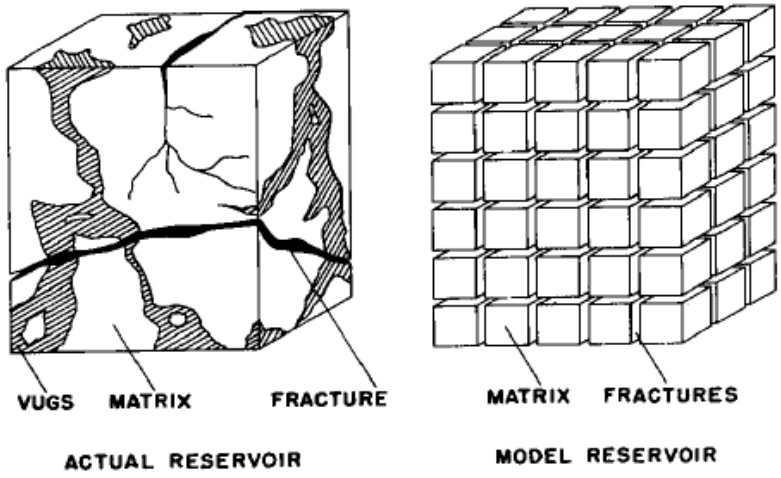

Figure 2.1: Idealization of the heterogeneous dual-porosity medium with uniform cubic matrix blocks (Warren and Root, 1963)

To couple the fluid flow between the matrix and the fracture with uniform matrix block idealization of fractured reservoirs, a transfer function is added to the continuity equation. The continuity equation for the ***single phase***, ***slightly compressible***, 1D flow in a dual-porosity media with ***uniform size***, ***homogeneous and isotropic matrix*** is given by:

$$\left(0.006328\frac{k_{f,eff}}{\mu}\right)\frac{\partial^2 \Delta p_f(x,t)}{\partial x^2} - \tau = \left(\phi c_t\right)_f \frac{\partial \Delta p_f(x,t)}{\partial t} \qquad [2.1]$$

Where:

$$\Delta p_f = p_i - p_{wf} \qquad [2.2]$$

2.2 Multiple-Matrix Model

In reality, the matrix blocks are not uniform and equally sized. In the dual-porosity reservoir of this research, each matrix block has its own size, permeability, and porosity, as illustrated in **Fig. 2.2**:

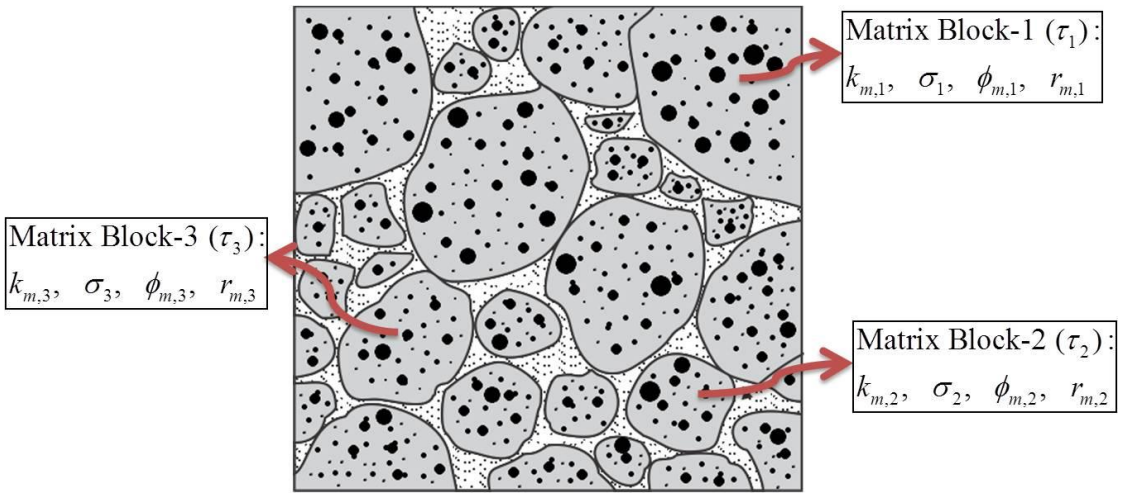

Figure 2.2: Schematic of a fractured dual-porosity medium with non-uniform matrix blocks

If statistically we have N_b different matrix blocks in a representative elementary volume, we arrive at the following diffusivity equation for 1D linear flow:

$$\left(0.006328\frac{k_{f,eff}}{\mu}\right)\frac{\partial^2 \Delta p_f(x,t)}{\partial x^2} - f_1\tau_1 - f_2\tau_2 - \ldots - f_{N_b}\tau_{N_b} = (\phi c_t)_f \frac{\partial \Delta p_f(x,t)}{\partial t} \qquad [2.3]$$

Where f_1, f_2, ..., f_{Nb} are volume fraction contributions for each matrix block in the representative elementary volume (REV) used in the analytical solutions or in the control volume (CV) of numerical solutions. The summation of these volume fractions must be 1, as shown by **Eq. 2.4**.

$$\sum_{i=1}^{N_b} f_i = 1; \quad (i = 1,2,...,N_b) \qquad [2.4]$$

Although I only presented the single-phase, 1D fluid flow equation for multiple-matrix setting, it can be applied for multi-phase, multi-component flow problems with the higher heterogeneity of the matrix blocks such as assigning different PVT data sets for each matrix blocks.

CHAPTER 3
MATRIX-FRACTURE TRANSFER FUNCTIONS

In this chapter, I present the pseudo-steady state and unsteady state matrix-fracture transfer functions for both uniform matrix blocks and the matrix blocks having different geometric shapes and properties. I start with the derivation of pseudo-steady state transfer function for single phase flow. Then, I present the unsteady-state transfer functions for sphere, slab and cuboid matrix blocks. Here I show the basic steps of the derivation, however, full derivation of unsteady-state transfer functions can be found in Appendix A. The transfer functions presented in this chapter are going to be used in both the analytical and numerical solutions in the next chapters.

3.1 Pseudo-Steady State Transfer Functions

The dual porosity diffusivity equation considers the conservation of mass in the fracture. The transfer function in **Eq. 2.1**, reflects the volume of fluid transferred from matrix to the fracture per unit rock volume per unit time. If I consider the conservation of mass principle in the matrix system, I can write:

$$\tau = \left(\phi c_t\right)_m \frac{\partial p_m}{\partial t} \qquad [3.1]$$

The relationship between the conservation of mass principle and fluid flow between matrix and fracture can be obtained from the Darcy's law. The transfer function representing the fluid transfer between fracture and the surrounding rock matrix for single-phase flow is:

$$\tau = \left(\sigma \frac{k_m}{\mu}\right)\left(p_f - p_m\right) \qquad [3.2]$$

If we combine **Eqs. 3.1** and **3.2**, we get:

$$\left(\sigma \frac{k_m}{\mu}\right)\left(p_f - p_m\right) = \left(\phi c_t\right)_m \frac{\partial p_m}{\partial t} \qquad [3.3]$$

Where the shape factor, σ, for a cuboid matrix block with dimensions L_x, L_y and L_z is:

$$\sigma = 4\left[\frac{1}{L_x^2} + \frac{1}{L_y^2} + \frac{1}{L_z^2}\right] \qquad [3.4]$$

The definition of the pseudo-steady state transfer function is independent from the shape of the matrix blocks, however, the shape factor has different definitions for the matrix blocks having different geometry.

3.2 Unsteady State Transfer Functions

As stated before, the fluid transfer from shale matrix blocks to the fractures takes a long time to reach pseudo-steady state regime because of the extremely tight nature of the matrix blocks. Thus, I first focused on formulating the transfer function to model the transient fluid flow between fracture and matrix. My derivation of unsteady state (USS) transfer functions, for different geometric shapes, followed the formulation provided by de Swaan-O in 1976 (shown below):

$$\tau(x,t) = \frac{2}{A_m w_f} \int_0^t \frac{\partial \Delta p_f(x,t)}{\partial \xi} q_{u,m}(t-\xi)\, d\xi \qquad [3.5]$$

Figure 3.1 compares the pressure drops of PSS and USS transfer function models for an example problem. As shown in the figure, the early time and the late time responses don't match each other. This is because of an error in deSwaan's USS transfer function formulation. The USS transfer function must represent the flow rate of fluid transfer between matrix and fracture per unit ***total*** rock volume containing fracture and matrix. However, de Swaan-O's USS transfer function definition reflects the flow rate of fluid transfer per unit ***fracture*** volume.

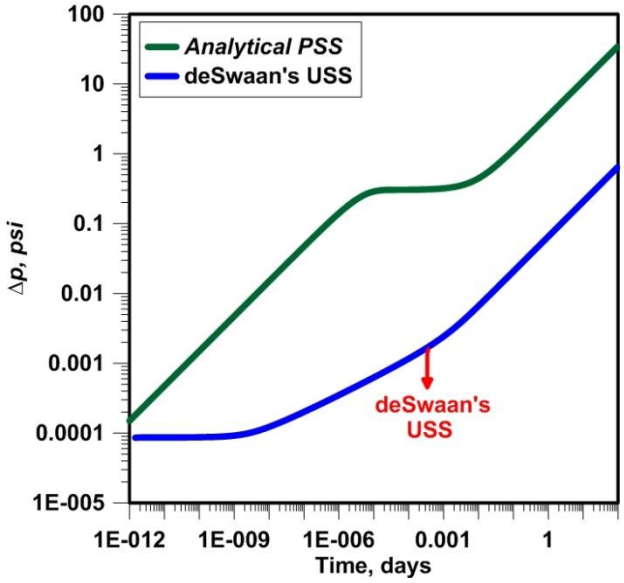

Figure 3.1: Comparison of pressure responses of PSS and de Swaan-O's USS models

The new ***unsteady-state (USS) transfer function***, τ which represents the flow rate of fluid transfer between fracture and matrix per unit rock volume, is given below:

$$\tau(x,t)=\frac{1}{V_m}\int_0^t \frac{\partial \Delta p_f(x,t)}{\partial \xi} q_{u,m}(t-\xi)\,d\xi \qquad [3.6]$$

Where, $q_{u,m}$ is the ***flow rate caused by a unit pressure drop at the matrix surface***. For a spherical matrix, $q_{u,m}$ is given by the following equation:

$$q_{u,m}(x,t)=-0.006328\frac{k_m}{\mu}A_m\left.\frac{\partial \Delta p_m(r,t;x)}{\partial r}\right|_{r=r_m} \qquad [3.7]$$

I begin to illustrate the use of **Eq. 3.6** by assuming that the matrix blocks are spheres and surrounded by fractures. The ***pressure change*** at any point, *r*, in such a ***sphere***, when the surface pressure p_m is suddenly decreased by 1 unit of pressure, is given below (adopted from the heat conduction problem by Carslaw and Jaeger, 1959):

$$\Delta p_m(r,t;x)=1+\left(\frac{2r_m}{\pi}\right)\frac{1}{r}\sum_{n=1}^{\infty}\frac{(-1)^n}{n}\exp\left(\frac{-\eta_m n^2\pi^2 t}{r_m^2}\right)\sin\left(\frac{n\pi r}{r_m}\right) \qquad [3.8]$$

Where:

$$\eta_m=\frac{0.006328k_m}{(\phi\mu c_t)_m} \qquad [3.9]$$

$$\Delta p_m=p_m^o-p_m \qquad [3.10]$$

$$\Delta p_m(r=r_m)=1\ psi \qquad [3.11]$$

Thus, for the ***spherical matrix block***, the transient transfer function becomes:

$$\tau(x,t)=0.006328\frac{k_m}{\mu}\sigma\frac{6}{\pi^2}\int_0^t \frac{\partial \Delta p_f(x,t)}{\partial \xi}\left[\sum_{n=1}^{\infty}\exp\left(-\eta_m n^2\sigma(t-\xi)\right)\right]d\xi \qquad [3.12]$$

Where σ is the ***shape factor*** for a ***spherical matrix block*** as shown:

$$\sigma=\pi^2/r_m^2 \qquad [3.13]$$

I also consider slab and cuboid (cuboid means rectangular cuboid in this thesis) for the shape of the matrix blocks and present the unsteady-state transfer functions for these shapes (for derivations see Appendix A). For a ***slab matrix block***, the transfer function is:

$$\tau(x,t) = 0.006328 \frac{k_m}{\mu} \sigma \frac{8}{\pi^2} \int_0^t \frac{\partial \Delta p_f(x,t)}{\partial \xi} \left[\sum_{n=0}^{\infty} \exp\left(-\eta_m (2n+1)^2 \sigma (t-\xi) \right) \right] d\xi \qquad [3.14]$$

Where σ is the ***shape factor*** for a ***slab matrix*** block, given below:

$$\sigma = \pi^2 / L_z^2 \qquad [3.15]$$

And for a ***cuboid matrix block*** the transfer function takes the following form:

$$\tau(x,t) = 0.006328 \frac{k_m}{\mu} \frac{512}{\pi^6} \int_0^t \frac{\partial \Delta p_f(x,t)}{\partial \xi} \left[\sum_{l=0}^{\infty} \sum_{m=0}^{\infty} \sum_{n=0}^{\infty} \frac{\pi^2 \left(\frac{(2l+1)^2}{L_x^2} + \frac{(2m+1)^2}{L_y^2} + \frac{(2n+1)^2}{L_z^2} \right)}{(2l+1)^2 (2m+1)^2 (2n+1)^2} \exp\left[-\eta_m \pi^2 \left(\frac{(2l+1)^2}{L_x^2} + \frac{(2m+1)^2}{L_y^2} + \frac{(2n+1)^2}{L_z^2} \right) (t-\xi) \right] \right] d\xi \qquad [3.16]$$

Where σ is the ***shape factor*** for a ***cuboid matrix block***:

$$\sigma = \pi^2 \left[\frac{1}{L_x^2} + \frac{1}{L_y^2} + \frac{1}{L_z^2} \right] \qquad [3.17]$$

CHAPTER 4

LAPLACE DOMAIN ANALYTICAL SOLUTIONS FOR PSS AND USS TRANSFER FUNCTIONS

In this chapter, I present the ***Laplace domain analytical solutions for constant terminal rate*** and ***constant terminal pressure***, both for single and multiple matrices using both the pseudo-steady state and unsteady state transfer functions. I evaluated these solutions in the Laplace domain and then numerically inverted the results into real time domain using numerical inverse of the Laplace transform (Stehfest, 1970).

4.1 Laplace Domain Solutions for Pseudo-Steady State Transfer Functions

I first present the analytical solutions for pseudo-steady state fluid transfer model. To develop the solutions, I used the transfer function presented in **Section 3.1**.

4.1.1 Solutions for Single-matrix Problem

The diffusivity equation for single-phase, slightly compressible, linear flow in a dual-porosity medium with uniform matrix block distribution is:

$$\left(0.006328\frac{k_{f,eff}}{\mu}\right)\frac{\partial^2 \Delta p_f(x,t)}{\partial x^2} - \tau = \left(\phi c_t\right)_f \frac{\partial \Delta p_f(x,t)}{\partial t} \qquad [4.1]$$

Where the transfer function is:

$$\tau = \lambda\left(\Delta p_f - \Delta p_m\right) \qquad [4.2]$$

And

$$\lambda\left(\Delta p_f - \Delta p_m\right) = \left(1-\omega\right)\frac{\partial \Delta p_m}{\partial t_D} \qquad [4.3]$$

Here, λ is ***inter porosity flow parameter*** and ω is ***fracture storativity ratio***. The mathematical definitions of λ and ω are:

$$\lambda = \sigma\frac{k_m}{k_{f,eff}}L^2 \qquad [4.4]$$

$$\omega = \frac{\left(\phi c_t\right)_f}{\left(\phi c_t\right)_f + \left(\phi c_t\right)_m} \qquad [4.5]$$

The dimensionless form of the diffusivity equation is:

$$\frac{\partial^2 p_{Df}}{\partial x_D^2} - \lambda\left(p_{Df} - p_{Dm}\right) = \omega\frac{\partial p_{Df}}{\partial t_D} \quad [4.6]$$

Where:

$$x_D = \frac{x}{W} \quad [4.7]$$

$$t_D = \frac{\left(0.006328\right)k_{f,eff}t}{\left[\left(\phi c_t\right)_f + \left(\phi c_t\right)_m\right]\mu L^2} \quad [4.8]$$

$$p_{Df}\left(t_D\right) = \frac{k_{f,eff}h}{141.2qB\mu}\left[p_f^o - p_f\left(t\right)\right] \quad [4.9]$$

Taking the Laplace transform of **Eqs. 4.3** and **4.6**, and combining them, I have:

$$\frac{d^2\Delta\bar{p}_{Df}\left(x_D\right)}{dx_D^2} - g\left(s\right)\Delta\bar{p}_{Df}\left(x_D\right) = 0 \quad [4.10]$$

And the g(s) function is:

$$g\left(s\right) = s\frac{\lambda + \left(1-\omega\right)\omega s}{\left(1-\omega\right)s + \lambda} \quad [4.11]$$

The wellbore pressure solution for this 1D, single-phase flow problem is:

$$\bar{p}_{Df}\left(s\right) = \frac{2\pi}{s\sqrt{g\left(s\right)}} \quad [4.12]$$

4.1.2 Solutions for Multiple-matrix Problem

The pseudo steady state transfer function representing the flow rate of fluid transfer from each matrix block in a multiple-matrix model is:

$$\tau_i = \sigma_i\frac{k_{m,i}}{\mu}\left(p_f - p_{m,i}\right); \quad i = 1,2,...,N_b \quad [4.13]$$

And

$$\sigma_i \frac{k_{m,i}}{\mu}\left(p_f - p_{m,i}\right) = \left(\phi c_t\right)_{m,i} \frac{\partial p_{m,i}}{\partial t}; \quad i = 1,2,...,N_b \tag{4.14}$$

The wellbore pressure solution in the Laplace domain for this problem is as single-matrix solution, as shown below:

$$\bar{p}_{Df}\left(s\right) = \frac{2\pi}{s\sqrt{g\left(s\right)}} \tag{4.15}$$

However, the g(s) function has a modified form to capture the flow contributions from non-uniform matrix blocks, **Eq. 4.16**:

$$g\left(s\right) = s\left[f_1\left(\frac{\lambda_1 + \left(1-\omega\right)\omega s}{\left(1-\omega\right)s + \lambda_1} \right) + f_2\left(\frac{\lambda_2 + \left(1-\omega\right)\omega s}{\left(1-\omega\right)s + \lambda_2} \right) + ... + f_{N_b}\left(\frac{\lambda_{N_b} + \left(1-\omega\right)\omega s}{\left(1-\omega\right)s + \lambda_{N_b}} \right) \right] \tag{4.16}$$

4.2 Laplace Domain Solutions for Unsteady State Transfer Functions

This section presents the Laplace domain analytical solutions for unsteady state transfer functions presented from **Eq. 3.11** to **3.15**. I developed the solutions for only spherical matrix blocks, however, similar solutions can be derived for cuboid and slab matrix blocks by following the similar procedures.

4.2.1 Solutions for Single-matrix Problem

The 1D dual-porosity pressure solution at the any point x, for constant terminal rate, in the Laplace domain, is (for full derivation, see appendix B):

$$\Delta\bar{p}_f\left(x,s\right) = \frac{1}{s\sqrt{g\left(s\right)}} \frac{qB\mu}{0.006328 k_{f,eff} hL} \exp\left(-\sqrt{g\left(s\right)}\, x\right) \tag{4.17}$$

And for x=0, the pressure solution at the wellbore intersected by an axial vertical fracture is:

$$\Delta\bar{p}_f\left(0,s\right) = \frac{1}{s\sqrt{g\left(s\right)}} \frac{qB\mu}{0.006328 k_{f,eff} hL} \tag{4.18}$$

Where, the *g(s)* function in the Laplace domain for uniform spherical matrix blocks is:

$$g(s) = s\left[\frac{(\varphi\mu c_t)_f}{0.006328 k_{f,eff}} + \frac{k_m}{k_{f,eff}}\sigma\frac{6}{\pi^2}\sum_{n=1}^{\infty}\frac{1}{s+\sigma\eta_m n^2}\right] \quad [4.19]$$

Similarly, flow rate vs. time solutions for the ***constant terminal pressure case*** can be obtained. For instance the bottom-hole flow rate solution in the Laplace-domain is:

$$\bar{q}B = 0.006328\frac{k_{f,eff}}{\mu}hL\,\Delta p_f\big|_{x=0}\left(\frac{\sqrt{g(s)}}{s}\right) \quad [4.20]$$

After inverting **Eq. 4.18** for the USS fluid transfer model, I compared the results with the ***numerical*** and ***analytical pseudo-steady-state (PSS)*** dual-porosity models. For analytical PSS model, I used the Laplace domain solution and calculated the pressure response in the Laplace domain. Then, I used numerical Laplace inversion to get the real time domain solutions. The numerical PSS results were generated by using the finite-difference numerical solution method. **Fig. 4.1** is a comparison of the USS analytical pressure solution with the numerical and analytical PSS pressure solutions. The USS dual-porosity model presented in this thesis generates the same pressure drops as the analytical and numerical PSS dual-porosity models for early and late time periods. The solution difference in the intermediate times is because of the difference in the formulation of USS and PSS models. I emphasize that the USS formulation is physically a more realistic model.

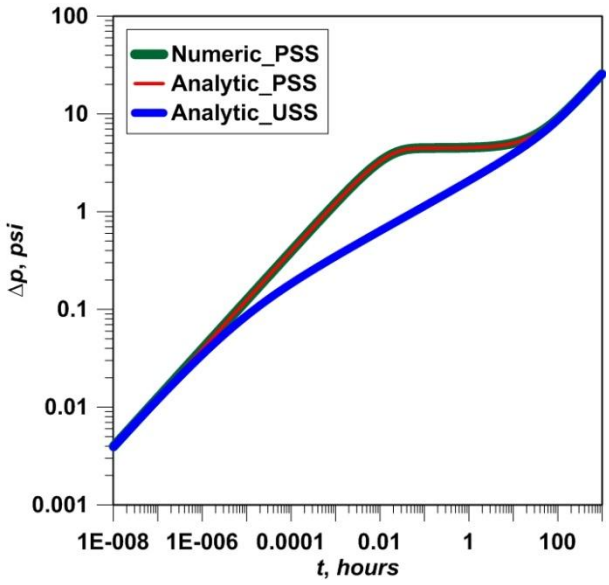

Figure 4.1: Comparison of dual-porosity model pressure responses

Fig. 4.2 presents a comparison of pressure derivative for USS and PSS models. Both the analytical and numerical pseudo-steady state (PSS) models show the V-shape characteristic of pseudo-steady state model. However, the unsteady-state model doesn't have the V-shape character.

The pressure transient studies presented in this thesis indicate that the classical pseudo-steady-state (PSS) V-shape characteristic of the pressure derivative plot for dual-porosity reservoirs is unrealistic, especially for unconventional reservoirs.

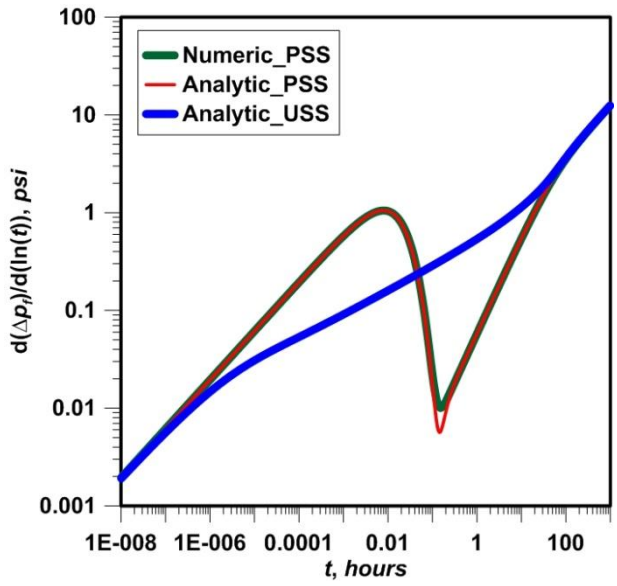

Figure 4.2: Comparison of dual-porosity model pressure-derivative responses

4.2.2 Solutions for Multiple-matrix Problems

The analytical solutions of the dual-porosity problems are based on the assumption that the matrix blocks are uniform throughout the reservoir. However, in this thesis, I deal with non-uniformity and heterogeneity of matrix blocks. In my formulation, the Laplace domain analytical solutions for the multiple-matrix model are same as the solutions for the uniform matrix block case but the $g(s)$ function is different.

For ***N_b non-uniform spherical matrix blocks***, the $g(s)$ function has the following form:

$$g(s)=s\left[\frac{(\phi\mu c_t)_f}{0.006328k_{f,eff}}+\left\{\begin{array}{l} f_1\frac{k_{m,1}}{k_{f,eff}}\sigma_1\frac{6}{\pi^2}\sum_{n=1}^{\infty}\frac{1}{s+\sigma_1\eta_{m,1}n^2}+f_2\frac{k_{m,2}}{k_{f,eff}}\sigma_2\frac{6}{\pi^2}\sum_{n=1}^{\infty}\frac{1}{s+\sigma_2\eta_{m,2}n^2} \\ +\ldots+f_{N_b}\frac{k_{m,N_b}}{k_{f,eff}}\sigma_{N_b}\frac{6}{\pi^2}\sum_{n=1}^{\infty}\frac{1}{s+\sigma_{N_b}\eta_{m,N_b}n^2}\end{array}\right\}\right] \quad [4.21]$$

The matrix volumetric average pressures in each matrix blocks can be calculated using the following equation in the Laplace-domain:

$$\Delta\bar{p}_{m,i}(x,s)=\frac{0.006328k_{m,i}}{(\phi c_t)_{m,i}\,\mu}\sigma_i\frac{6}{\pi^2}\Delta\bar{p}_f(x,s)\sum_{n=1}^{\infty}\frac{1}{s+\sigma_i\eta_{m,i}n^2};\quad (i=1,2,\ldots,N_b) \quad [4.22]$$

To show the flow contributions of different matrix blocks, I ran the multiple-matrix model for two cases with three different matrix blocks. **Table 4.1** shows the input data for the first example problem. I considered three different matrix permeabilities: $1x10^{-5}$ *md*, $5x10^{-6}$ *md* and $1x10^{-6}$ *md*. The matrix blocks were spheres and the radii were also different: 0.5 *ft*, 1.0 *ft* and 5.0 *ft*. The volume fractions were 0.10, 0.10 and 0.80. **Fig. 4.3** shows the pressure drops in the fracture and each matrix block. The time required for matrix block-1 to reach the pseudo-steady state regime is about 0.4 day, while for second and third matrix blocks is 2 and 100 days, respectively. This clearly shows that increasing matrix block size and decreasing matrix permeability decreases the matrix contribution to flow.

TABLE 4.1 – INPUT DATA FOR TRIPLE-MATRIX EXAMPLE-1

Reservoir, Well, Fluid Properties			Matrix Block-1	Matrix Block-2	Matrix Block-3
μ *(cp)*	0.02	k_m *(md)*	$1x10^{-5}$	$5x10^{-6}$	$1x10^{-6}$
B (RCF/SCF)	1	φ_m	0.15	0.20	0.10
$c_{t,m}$ *(1/psi)*	$1.5x10^{-4}$	σ *(1/ft²)*	39.47	9.87	0.395
$c_{t,f}$ *(1/psi)*	$5x10^{-4}$	r_m *(ft)*	0.5	1	5
h (ft)	30	*f (fraction)*	0.1	0.1	0.8
L (ft)	5000				
φ_f	$3.94x10^{-5}$				
$k_{f,eff}$ *(md)*	$8.3x10^{-4}$				
q (SCF/D)	1000				

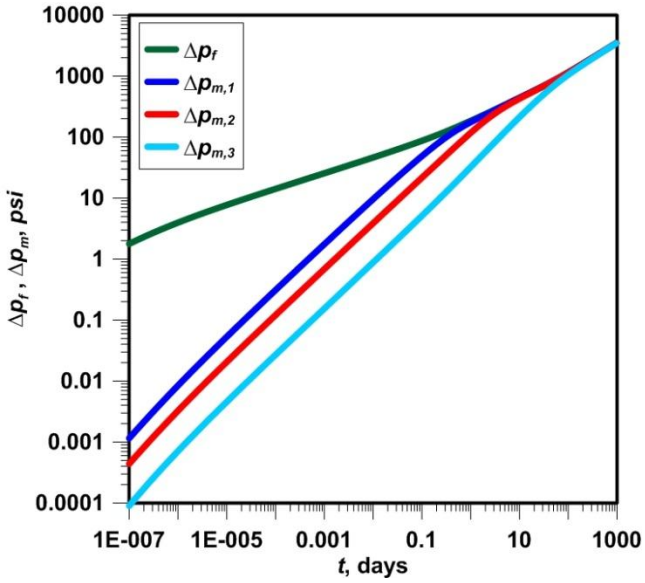

Figure 4.3: Pressure drops in fracture and each matrix block for triple-matrix Example 1

In the second example (**Table 4.2**), I used a fixed matrix porosity, 0.10, to see the effects of matrix size and permeability on the pressure drop in each matrix block. In this example, the matrix blocks were again spheres and the radii were 1.0 *ft*, 3.0 *ft* and 5.0 *ft*. I used the same matrix permeabilities: $1x10^{-5}$ *md*, $5x10^{-6}$ *md* and $1x10^{-6}$ *md*. The volume fraction of the first matrix block is 0.8, and the second and third matrix blocks have 0.1 for volume fractions.

TABLE 4.2 – INPUT DATA FOR TRIPLE-MATRIX EXAMPLE-2

Reservoir, Well, Fluid Properties				Matrix Block-1	Matrix Block-2	Matrix Block-3
μ *(cp)*	0.02	k_m *(md)*		$1x10^{-5}$	$5x10^{-6}$	$1x10^{-6}$
B *(RCF/SCF)*	1	φ_m		0.10	0.10	0.10
$c_{t,m}$ *(1/psi)*	$1.5x10^{-4}$	σ	*(1/ft²)*	9.87	1.096	0.395
$c_{t,f}$ *(1/psi)*	$5x10^{-4}$	r_m	*(ft)*	1	3	5
h *(ft)*	30	f	*(fraction)*	0.8	0.1	0.1
L *(ft)*	5000					
φ_f	$2x10^{-4}$					
$k_{f,eff}$ *(md)*	$8.3x10^{-4}$					
q *(SCF/D)*	1000					

Fig. 4.4 shows the resulting pressure drops in the fracture and in each matrix block. Similar to the previous example, the matrix block, which has the lowest permeability and largest diameter, requires

longer time to reach the pseudo-steady state flow regime. This clearly indicates that the property of one matrix block in a multiple-matrix system affects the pressure responses of other matrix blocks.

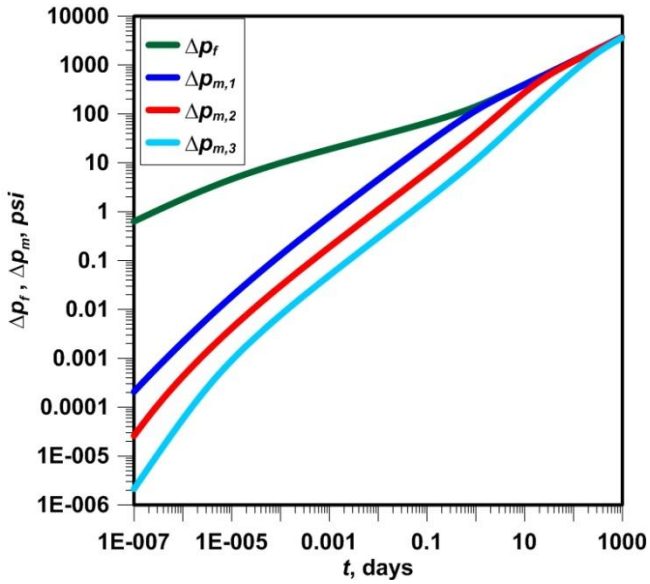

Figure 4.4: Pressure drops in fracture and each matrix block for triple-matrix Example 2

CHAPTER 5
EXTENSION OF SINGLE-PHASE THEORY TO WATER-OIL FLOW

The equations for the multi-phase, multi-component flow problems are highly non-linear, thus the analytical solutions for these non-linear systems are not present. However, for an approximation, I show the application of multiple-matrix model to the Buckley-Leverett (B-L) displacement, a quasi-linear form of multi-phase flow in dual-porosity reservoirs. The linearized B-L displacement in the fracture for a dual-porosity system with unsteady state transfer function was first presented by de Swaan-O (1978):

$$-u_{t,f}\frac{\partial S_{wf}(x,t)}{\partial x}-\frac{\tau}{\phi_f}=\frac{\partial S_{wf}(x,t)}{\partial t} \qquad [5.1]$$

Here τ is the ***unsteady state*** (USS) transfer function for water entering the matrix (or, equivalently, oil leaving the matrix):

$$\tau=\tilde{\lambda}R_{\infty}\int_0^t e^{-\tilde{\lambda}(t-\xi)}\frac{\partial S_{wf}(x,t)}{\partial \xi}d\xi \qquad [5.2]$$

Laboratory experiments indicate that, the cumulative oil recovery by water imbibition and/or gravity drainage from matrix can be approximated by the following exponential curve (Kazemi, et al., 1992):

$$R=R_{\infty}\left(1-e^{-\tilde{\lambda}t}\right) \qquad [5.3]$$

Where, R_{∞} is ***the maximum oil volume recovered per unit rock volume at infinite time*** and R is ***the oil volume recovered per unit rock volume at any time t***. The exponential decline parameter, $\tilde{\lambda}$, can be calculated by matching experimental data using **Eq. 1.3**. The calculated exponential decline parameter includes the combined effects of viscous, capillary and gravity forces for the specific rock sample. The Laplace domain solution of the water saturation at any point (*x*, *t*) in the fracture space for a single-matrix is:

$$\bar{S}_{wf}(x,s)=\frac{1}{s}\exp\left(-\frac{s}{u_{t,f}}\left(\frac{\tilde{\lambda}R_{\infty}}{\phi_f}\frac{1}{s+\tilde{\lambda}}+1\right)x\right) \qquad [5.4]$$

If we have multiple-matrices in each representative elementary volume (REV), the water-oil displacement equation, **Eq. 5.1**, becomes:

$$-u_{t,f}\frac{\partial S_{wf}\left(x,t\right)}{\partial x}-f_1\frac{\tau_1}{\phi_f}-f_2\frac{\tau_2}{\phi_f}-...-f_{N_b}\frac{\tau_{N_b}}{\phi_f}=\frac{\partial S_{wf}\left(x,t\right)}{\partial t} \quad [5.5]$$

The *unsteady-state transfer function* for each matrix block is:

$$\tau_i=\tilde{\lambda}_i R_{\infty,i}\int_0^t e^{-\tilde{\lambda}_i(t-\xi)}\frac{\partial S_{wf}\left(x,t\right)}{\partial \xi}d\xi\,;\quad \left(i=1,2,...,N_b\right) \quad [5.6]$$

In this multiple-matrix setting, each matrix block may have its own mass transfer coefficient ($\tilde{\lambda}_i$) and ultimate recovery per unit rock volume ($R_{\infty,i}$). The water saturation in the fracture for multiple-matrix model in the Laplace-domain is:

$$\bar{S}_{wf}\left(x,s\right)=\frac{1}{s}\exp\left(-\frac{s}{u_{t,f}}\left(\begin{array}{l} f_1\dfrac{\tilde{\lambda}_1 R_{\infty,1}}{\phi_f}\dfrac{1}{s+\tilde{\lambda}_1}+f_2\dfrac{\tilde{\lambda}_2 R_{\infty,2}}{\phi_f}\dfrac{1}{s+\tilde{\lambda}_2}+...+ \\ f_{N_b}\dfrac{\tilde{\lambda}_{N_b} R_{\infty,N_b}}{\phi_f}\dfrac{1}{s+\tilde{\lambda}_{N_b}}+1 \end{array}\right)x\right) \quad [5.7]$$

The solution of **Eq. 5.7** is reserved for the extension of this thesis to a PhD research plan.

CHAPTER 6
CLOSED FORM SOLUTIONS FOR PRESSURE TRANSIENT TEST ANALYSIS WITH USS TRANSFER FUNCTION

To derive the closed form solutions for both single- and multiple-matrix model for interpretation of the pressure transient test data, I present the formulation in terms of dimensionless parameters. The dimensionless diffusivity equation in the Laplace-domain is:

$$\frac{\partial^2 \bar{p}_{Df}}{\partial x_D^2} = g(s)\,\bar{p}_{Df} \qquad [6.1]$$

6.1 Closed-Form Solutions for Single-Matrix Model

The diffusivity equation for single phase, slightly compressible linear fluid flow in a dual porosity medium with uniform matrix block distribution is:

$$(0.006328)\frac{k_{f,eff}}{\mu}\frac{\partial^2 \Delta p_f}{\partial x^2} - \tau = (\phi c_t)_f \frac{\partial \Delta p_f}{\partial t} \qquad [6.2]$$

I need to define the dimensionless parameters to write the diffusivity equation (**Eq 6.2**) in dimensionless form:

$$x_D = \frac{x}{L} \qquad [6.3]$$

$$t_D = \frac{(0.006328)k_{f,eff}t}{\left[(\phi c_t)_f + (\phi c_t)_m\right]\mu L^2} \qquad [6.4]$$

$$p_{Df}(t_D) = \frac{k_{f,eff}h}{141.2qB\mu}\left[\Delta p_f(t)\right] \qquad [6.5]$$

By using these dimensionless variables, I obtain the dimensionless diffusivity equation as following (for full derivation, see Appendix B):

$$\frac{\partial^2 \bar{p}_{Df}}{\partial x_D^2} = \left[\omega + \frac{3}{\pi}\sqrt{\frac{\lambda(1-\omega)}{s}}\coth\left(\pi\sqrt{\frac{1-\omega}{\lambda}s}\right) - \frac{3}{\pi^2}\frac{\lambda}{s}\right]s\bar{p}_{Df} \qquad [6.6]$$

Where:

$$g(s)=s\left[\omega+\frac{3}{\pi}\sqrt{\frac{\lambda(1-\omega)}{s}}\coth\left(\pi\sqrt{\frac{1-\omega}{\lambda}s}\right)-\frac{3}{\pi^2}\frac{\lambda}{s}\right] \quad [6.7]$$

The wellbore pressure solution in the Laplace domain for this problem is given as following:

$$\bar{p}_{Df}(s)=\frac{2\pi}{s\sqrt{g(s)}} \quad [6.8]$$

6.1.1 Early Time Closed-Form Solution

In early times, because the time is very small, the Laplace transform variable *s* becomes very large. Thus the *g*(*s*) function reduces to:

$$g(s)=s\omega \quad [6.9]$$

The wellbore pressure solution in the Laplace domain becomes:

$$\bar{p}_{Df}(s)=\frac{2\pi}{s^{3/2}\sqrt{\omega}} \quad [6.10]$$

Inverting into the real time domain, I obtain:

$$p_{Df}(t)=4\sqrt{\frac{\pi}{\omega}t_D} \quad [6.11]$$

In dimensional form, the early time pressure solution for a ***two-sided reservoir model*** is:

$$\Delta p_f(t)=\frac{8.128qB\mu}{\sqrt{k_{f,eff}}hL}\left(\frac{1}{(\phi\mu c_t)_f}\right)^{1/2}\sqrt{t} \quad [6.12]$$

Please note that, in the above solution, the flow rate is in *STB/D* and the time is in *hours*.

6.1.2 Intermediate Time Closed-Form Solution

The intermediate time flow regime follows the early time fracture flow and matrix starts to feed the reservoir in this flow period. Thus, to obtain the closed-form solution for intermediate flow regime, fracture storativity can be ignored. For intermediate times, *g*(*s*) function can be approximated (for x>3.6, coth(x)≈1) :

$$g(s) = s\left(\frac{3}{\pi}\sqrt{\frac{\lambda(1-\omega)}{s}}\right) \quad [6.13]$$

The wellbore pressure solution in the Laplace domain becomes:

$$\bar{p}_{Df}(s) = \frac{2\pi}{s^{5/4}\sqrt{\frac{3}{\pi}\sqrt{\lambda(1-\omega)}}} \quad [6.14]$$

Inverting into the real time domain yields:

$$p_{Df}(t_D) = \frac{t_D^{1/4}}{\Gamma\left(5/4\right)}\frac{2\pi}{\sqrt{\frac{3}{\pi}\sqrt{\lambda(1-\omega)}}} \quad [6.15]$$

Under this assumption, I arrive at the closed-form pressure solution for intermediate-time (the flow rate is in STB/D and the time is in hour):

$$\Delta p_f(t) = \frac{(63.82)qB\mu}{\sqrt{k_{f,eff}}hL}\left(\frac{1}{\sigma k_m(\phi\mu c_t)_m}\right)^{1/4} t^{1/4} \quad [6.16]$$

And the effective permeability can be estimated from the slope of $\Delta p_f(t)$ vs $t^{1/4}$ plot, as following:

$$k_{f,eff} = \left(\frac{(63.82)qB\mu}{m_{\text{intermediate}}hL}\right)^2\left(\frac{1}{\sigma k_m(\phi\mu c_t)_m}\right)^{1/2} \quad [6.17]$$

6.1.3 Late Time Closed-Form Solution

In the late times, the reservoir acts like a single-porosity media. Thus, for late times, the *g*(*s*) function can be used as:

$$g(s) = s \quad [6.18]$$

The wellbore pressure solution in the Laplace domain becomes:

$$\bar{p}_{Df}(s) = \frac{2\pi}{s^{3/2}} \quad [6.19]$$

The real time domain inversion of the wellbore pressure solution is:

$$p_{Df}\left(t_D\right)=4\sqrt{\pi t_D} \qquad [6.20]$$

The closed-form solution for *late time flow regime* becomes:

$$\Delta p_f\left(t\right)=\frac{8.128qB\mu}{\sqrt{k_{f,eff}}hL}\left(\frac{1}{\left(\phi\mu c_t\right)_{f+m}}\right)^{1/2}\sqrt{t} \qquad [6.21]$$

The slope of $\Delta p_f\left(t\right)$ vs $t^{1/2}$ plot can be used to estimate the effective permeability from linear flow period:

$$k_{f,eff}=\left(\frac{8.128qB\mu}{m_{linear}hL}\right)^2\frac{1}{\left(\phi\mu c_t\right)_{f+m}} \qquad [6.22]$$

As an example, **Fig. 6.1** shows the single-matrix USS pressure and pressure derivative (logarithmic derivative) profiles for flow through a **5000-*ft horizontal well*** in a naturally fractured reservoir. The data used for the example problem are given in **Table 6.1**. Looking at the transition zone between the two linear flow periods, one can observe the absence of the V-shape feature of the classical pseudo-steady-state, dual-porosity model. The lack of such a V-shape feature is supported by field observations.

TABLE 6.1 – INPUT DATA FOR FLOW THROUGH A 5000-FT HORIZONTAL WELL

Reservoir, Well, Fluid Properties

μ	*(cp)*	0.02	k_m	*(md)*	1×10^{-5}
B	*(RB/STB)*	1	$k_{f,eff}$	*(md)*	2.8×10^{-4}
$c_{t,m}$	*(1/psi)*	5×10^{-4}	σ	*(1/ft²)*	4.1
$c_{t,f}$	*(1/psi)*	1.5×10^{-4}	r_m	*(ft)*	1.55
h	*(ft)*	100	φ_f		2×10^{-3}
L	*(ft)*	5000	φ_m		0.05
q	*(STB/D)*	356.2			

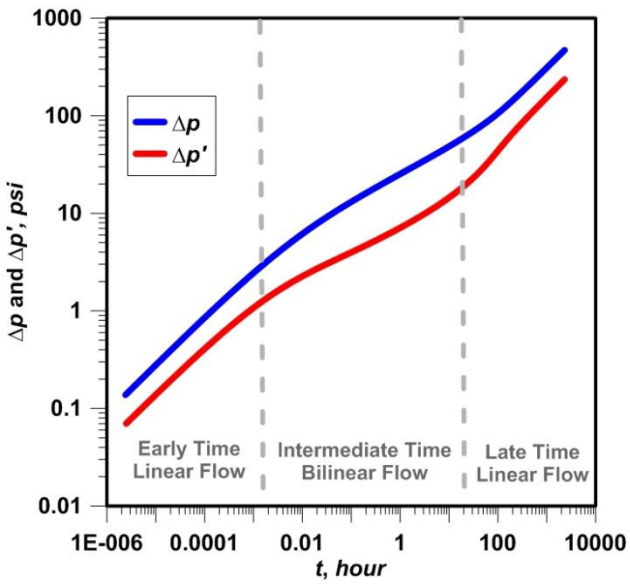

Figure 6.1: Pressure and logarithmic derivative of pressure for horizontal well example

I estimated the effective permebilities as $2.34\text{x}10^{-4}$ *md* and $2.82\text{x}10^{-4}$ *md* from the intermediate and late time flow solutions (**Eqs. 6.17** and **6.22**), respectively.

6.2 Closed-Form Solutions for Multiple-Matrix Model

The diffusivity equation for single phase, slightly compressible linear fluid flow in a dual porosity medium with non-uniform matrix block distribution is:

$$(0.006328)\frac{k_{f,eff}}{\mu}\frac{\partial^2 \Delta p_f}{\partial x^2} - f_1\tau_1 - f_2\tau_2 = (\phi c_t)_f \frac{\partial \Delta p_f}{\partial t} \qquad [6.23]$$

And the unsteady-state transfer functions are for each matrix block are:

$$\tau_i(x,t) = \frac{1}{V_{m,i}}\int_0^t \frac{\partial \Delta p_f(x,t)}{\partial \xi} q_{u,m,i}(t-\xi)\,d\xi; \quad (i = 1,2,...,N_b) \qquad [6.24]$$

The new definitions of dimensionless variables for MM setting are:

$$t_D = \frac{(0.006328)k_{f,eff}\,t}{\left[(\phi c_t)_f + f_1(\phi c_t)_{m,1} + f_2(\phi c_t)_{m,2} + ... + f_{N_b}(\phi c_t)_{m,N_b}\right]\mu L^2} \qquad [6.25]$$

$$\omega = \frac{(\phi c_t)_f}{\left[(\phi c_t)_f + f_1(\phi c_t)_{m,1} + f_2(\phi c_t)_{m,2} + ... + f_{N_b}(\phi c_t)_{m,N_b}\right]} \quad [6.26]$$

$$\lambda_i = \sigma_i \frac{k_{m,i}}{k_{f,eff}} L^2; \quad (i = 1,2,...,N_b) \quad [6.27]$$

By using these dimensionless variables, I obtain the dimensionless diffusivity equation for multiple-matrix model as following (for full derivation, see Appendix B):

$$\frac{\partial^2 \bar{p}_{Df}}{\partial x_D^2} = \begin{bmatrix} \omega + f_1\left[\frac{3}{\pi}\left(\sqrt{\frac{\lambda_1\omega}{F_1 s}}\coth\left(\pi\sqrt{\frac{\omega}{\lambda_1 F_1}s}\right) - \frac{1}{r_{m,1}s}\right)\right] \\ + f_2\left[\frac{3}{\pi}\left(\sqrt{\frac{\lambda_2\omega}{F_2 s}}\coth\left(\pi\sqrt{\frac{\omega}{\lambda_2 F_2}s}\right) - \frac{1}{r_{m,2}s}\right)\right] \\ \vdots \\ + f_{N_b}\left[\frac{3}{\pi}\left(\sqrt{\frac{\lambda_{N_b}\omega}{F_{N_b} s}}\coth\left(\pi\sqrt{\frac{\omega}{\lambda_{N_b} F_{N_b}}s}\right) - \frac{1}{r_{m,N_b}s}\right)\right] \end{bmatrix} s\bar{p}_{Df} \quad [6.28]$$

Where:

$$F_i = \frac{(\phi c_t)_f}{(\phi c_t)_{m,i}}; \quad (i = 1,2,...,N_b) \quad [6.29]$$

$$g(s) = s\begin{bmatrix} \omega + f_1\left[\frac{3}{\pi}\left(\sqrt{\frac{\lambda_1\omega}{F_1 s}}\coth\left(\pi\sqrt{\frac{\omega}{\lambda_1 F_1}s}\right) - \frac{1}{r_{m,1}s}\right)\right] \\ + f_2\left[\frac{3}{\pi}\left(\sqrt{\frac{\lambda_2\omega}{F_2 s}}\coth\left(\pi\sqrt{\frac{\omega}{\lambda_2 F_2}s}\right) - \frac{1}{r_{m,2}s}\right)\right] \\ \vdots \\ + f_{N_b}\left[\frac{3}{\pi}\left(\sqrt{\frac{\lambda_{N_b}\omega}{F_{N_b} s}}\coth\left(\pi\sqrt{\frac{\omega}{\lambda_{N_b} F_{N_b}}s}\right) - \frac{1}{r_{m,N_b}s}\right)\right] \end{bmatrix} \quad [6.30]$$

5.2.1 Early Time Closed-Form Solution

Because the early time flow is dominated by the fracture flow, I have the same early time solution with the single-matrix setting. The early time wellbore pressure solution is:

$$\Delta p_f(t) = \frac{8.128 qB\mu}{\sqrt{k_{f,eff}}hL}\left(\frac{1}{(\phi\mu c_t)_f}\right)^{1/2}\sqrt{t} \qquad [6.31]$$

6.2.2 Intermediate Time Closed-Form Solution

Similarly to the single-matrix solution, for intermediate times, the $g(s)$ function can be approximated as:

$$g(s) = s\begin{bmatrix} f_1\left[\frac{3}{\pi}\sqrt{\frac{\lambda_1\omega}{F_1 s}}\right] \\ +f_2\left[\frac{3}{\pi}\sqrt{\frac{\lambda_2\omega}{F_2 s}}\right] \\ \vdots \\ +f_{N_b}\left[\frac{3}{\pi}\sqrt{\frac{\lambda_{N_b}\omega}{F_{N_b} s}}\right] \end{bmatrix} \qquad [6.32]$$

The wellbore pressure solution in the Laplace domain becomes:

$$\bar{p}_{Df}(s) = \frac{2\pi}{s^{5/4}\sqrt{f_1\frac{3\lambda_1}{\pi}\sqrt{\frac{\omega}{\lambda_1 F_1}} + f_2\frac{3\lambda_2}{\pi}\sqrt{\frac{\omega}{\lambda_2 F_2}} + \ldots + f_{N_b}\frac{3\lambda_{N_b}}{\pi}\sqrt{\frac{\omega}{\lambda_{N_b}F_{N_b}}}}} \qquad [6.33]$$

Inverting into real time domain gives:

$$p_{Df}(t_D) = \frac{t_D^{1/4}}{\Gamma\left(5/4\right)}\frac{2\pi}{\sqrt{f_1\frac{3\lambda_1}{\pi}\sqrt{\frac{\omega}{\lambda_1 F_1}} + f_2\frac{3\lambda_2}{\pi}\sqrt{\frac{\omega}{\lambda_2 F_2}} + \ldots + f_{N_b}\frac{3\lambda_{N_b}}{\pi}\sqrt{\frac{\omega}{\lambda_{N_b}F_{N_b}}}}} \qquad [6.34]$$

And the closed-form pressure solution for intermediate-time in multiple-matrix setting is:

$$\Delta p_f(t) = \frac{(63.82)qB\mu}{\sqrt{k_{f,eff}}hL}\left(\frac{1}{\left[\begin{array}{l}\sqrt{f_1^2\sigma_1 k_{m,1}(\phi\mu c_t)_{m,1}} + \sqrt{f_2^2\sigma_2 k_{m,2}(\phi\mu c_t)_{m,2}} \\ +\ldots+\sqrt{f_{N_b}^2\sigma_{N_b} k_{m,N_b}(\phi\mu c_t)_{m,N_b}}\end{array}\right]}\right)^{1/2} t^{1/4} \qquad [6.35]$$

And the effective permeability for the multiple-matrix setting can be estimated from the slope of $\Delta p_f(t)$ vs $t^{1/4}$ plot, as shown in the following equation:

$$k_{f,eff} = \left(\frac{(63.82)qB\mu}{m_{bilinear}hL}\right)^2 \left(\frac{1}{\left[\begin{array}{l}\sqrt{f_1^2\sigma_1 k_{m,1}(\phi\mu c_t)_{m,1}} + \sqrt{f_2^2\sigma_2 k_{m,2}(\phi\mu c_t)_{m,2}} \\ +\ldots+\sqrt{f_{N_b}^2\sigma_{N_b} k_{m,N_b}(\phi\mu c_t)_{m,N_b}}\end{array}\right]}\right) \quad [6.36]$$

6.2.3 Late Time Closed-Form Solution

For multiple-matrix setting, I have the same late time approximation with single matrix setting, as shown by the following equation:

$$g(s) = s \quad [6.37]$$

And the wellbore pressure solution in the real time domain is:

$$p_{Df}(t_D) = 4\sqrt{\pi t_D} \quad [6.38]$$

Because the definition of dimensionless time is different, I have a slightly different late time closed-form solution for multiple-matrix setting:

$$\Delta p_f(t) = \frac{8.128qB\mu}{\sqrt{k_{f,eff}}hL}\left(\frac{1}{\mu\left[(\phi c_t)_f + f_1(\phi c_t)_{m,1} + f_2(\phi c_t)_{m,2} + \ldots + f_{N_b}(\phi c_t)_{m,N_b}\right]}\right)^{1/2}\sqrt{t} \quad [6.39]$$

The slope of $\Delta p_f(t)$ vs $t^{1/2}$ plot can be used to estimate the effective permeability from linear flow period:

$$k_{f,eff} = \left(\frac{8.128qB\mu}{m_{linear}hL}\right)^2 \frac{1}{\mu\left[(\phi c_t)_f + f_1(\phi c_t)_{m,1} + f_2(\phi c_t)_{m,2} + \ldots + f_{N_b}(\phi c_t)_{m,N_b}\right]} \quad [6.40]$$

I used the data set in **Table 4.1** to generate the synthetic data for the triple-matrix example and then I plot $\Delta p_f(t)$ vs $t^{1/4}$ for the bilinear flow regime period (**Fig. 6.2**), I calculated the effective permeability as $7.77\text{x}10^{-4}$ *md* which originally was $8.3\text{x}10^{-4}$ *md*.

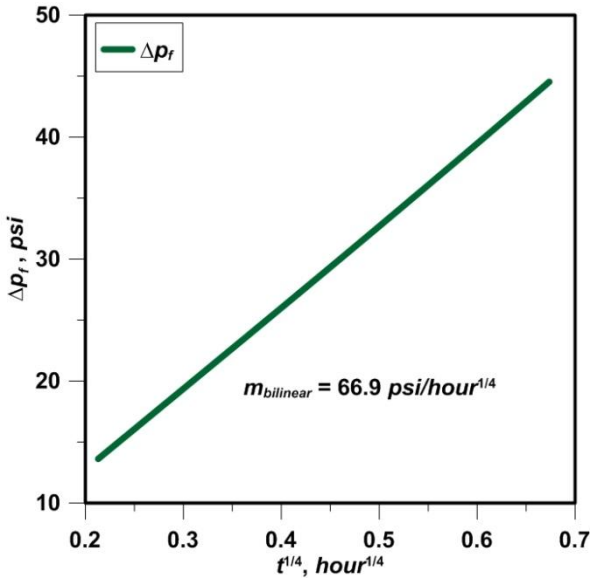

Figure 6.2: Pressure drop as a function of $t^{1/4}$ for *bilinear flow* analysis

CHAPTER 7

PRESSURE DISTRIBUTION IN A NANO-DARCY MATRIX BLOCK

The pressure distribution inside each matrix block can also be estimated by using the **MINC** (***Multiple Interacting Continua***) approach (Pruess and Narasimham, 1985). To estimate the pressure distribution, I divide the spherical matrix block into 3 segments having same volumes as shown in **Fig. 7.1**:

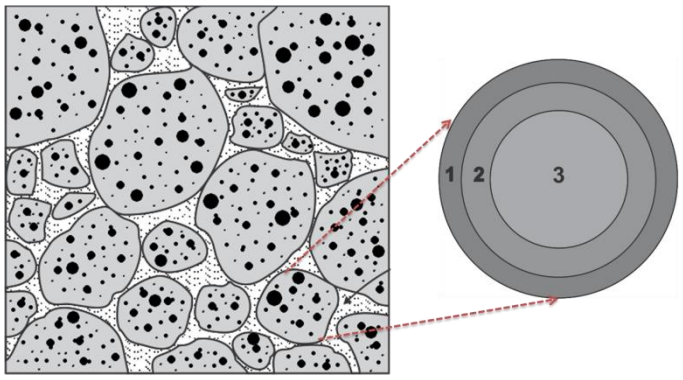

Figure 7.1: Schematic of equal volume rings inside a spherical matrix block

When I write the mass conservation equation between the transfer function and the three rings, I have three equations with three unknowns which are the pressure drops in each segment.

$$-\left(0.006328\right)\frac{k_m}{\mu}4\pi r_{m,3/2}^2\frac{\Delta p_{m,1}-\Delta p_{m,2}}{\Delta r_1}+V_m\tau=\left(\phi c_t\right)_m V_{m,1}\frac{\partial\Delta p_{m,1}}{\partial t} \quad [7.1]$$

$$\left(\begin{array}{l}-\left(0.006328\right)\frac{k_m}{\mu}4\pi r_{m,5/2}^2\frac{\Delta p_{m,2}-\Delta p_{m,3}}{\Delta r_2}\\+\left(0.006328\right)\frac{k_m}{\mu}4\pi r_{m,3/2}^2\frac{\Delta p_{m,1}-\Delta p_{m,2}}{\Delta r_1}\end{array}\right)=\left(\phi c_t\right)_m V_{m,2}\frac{\partial\Delta p_{m,2}}{\partial t} \quad [7.2]$$

$$\left(0.006328\right)\frac{k_m}{\mu}4\pi r_{m,5/2}^2\frac{\Delta p_{m,2}-\Delta p_{m,3}}{\Delta r_2}=\left(\phi c_t\right)_m V_{m,3}\frac{\partial\Delta p_{m,3}}{\partial t} \quad [7.3]$$

Taking the Laplace transform of mass conservation equations, respectively, yields:

$$-\left(0.006328\right)\frac{k_m}{\mu}4\pi r_{m,3/2}^2\frac{\Delta\bar{p}_{m,1}-\Delta\bar{p}_{m,2}}{\Delta r_1}+V_m\bar{\tau}=\left(\phi c_t\right)_m V_{m,1}s\Delta\bar{p}_{m,1} \quad [7.4]$$

$$\begin{pmatrix} -(0.006328)\dfrac{k_m}{\mu}4\pi r^2_{m,5/2}\dfrac{\Delta\bar{p}_{m,2}-\Delta\bar{p}_{m,3}}{\Delta r_2} \\ +(0.006328)\dfrac{k_m}{\mu}4\pi r^2_{m,3/2}\dfrac{\Delta\bar{p}_{m,1}-\Delta\bar{p}_{m,2}}{\Delta r_1} \end{pmatrix} = (\phi c_t)_m V_{m,2} s\Delta\bar{p}_{m,2} \qquad [7.5]$$

$$(0.006328)\frac{k_m}{\mu}4\pi r^2_{m,5/2}\frac{\Delta\bar{p}_{m,2}-\Delta\bar{p}_{m,3}}{\Delta r_2} = (\phi c_t)_m V_{m,3} s\Delta\bar{p}_{m,3} \qquad [7.6]$$

To solve the above equation set, I form the following matrix-vector system:

$$\begin{bmatrix} \begin{pmatrix} -0.006328\dfrac{k_m 4\pi r^2_{m,3/2}}{\mu\Delta r_1} \\ -s(\phi c_t)_m V_{m,1} \end{pmatrix} & \begin{pmatrix} 0.006328\dfrac{k_m 4\pi r^2_{m,3/2}}{\mu\Delta r_1} \end{pmatrix} & 0 \\ \begin{pmatrix} 0.006328\dfrac{k_m 4\pi r^2_{m,3/2}}{\mu\Delta r_1} \end{pmatrix} & \begin{pmatrix} -0.006328\dfrac{k_m 4\pi r^2_{m,3/2}}{\mu\Delta r_1} \\ -0.006328\dfrac{k_m 4\pi r^2_{m,5/2}}{\mu\Delta r_2} \\ -s(\phi c_t)_m V_{m,2} \end{pmatrix} & \begin{pmatrix} 0.006328\dfrac{k_m 4\pi r^2_{m,5/2}}{\mu\Delta r_2} \end{pmatrix} \\ 0 & \begin{pmatrix} 0.006328\dfrac{k_m 4\pi r^2_{m,5/2}}{\mu\Delta r_2} \end{pmatrix} & \begin{pmatrix} -0.006328\dfrac{k_m 4\pi r^2_{m,5/2}}{\mu\Delta r_2} \\ -s(\phi c_t)_m V_{m,3} \end{pmatrix} \end{bmatrix} \begin{bmatrix} \Delta\bar{p}_{m,1} \\ \Delta\bar{p}_{m,2} \\ \Delta\bar{p}_{m,3} \end{bmatrix} = \begin{bmatrix} -V_m\bar{\tau} \\ 0 \\ 0 \end{bmatrix}$$

[7.7]

These matrix-vector system can be solved in the Laplace domain to get the pressure drops. A theoretical example case is presented below. The matrix blocks in this example were equally sized spheres. **Fig. 7.2** shows the average pressure drop in the spherical matrix block and the pressure drops in each region. The data used to construct **Fig. 7.2** are tabulated below.

TABLE 7.1 – INPUT DATA FOR PRESSURE DISTRIBUTION IN A MATRIX BLOCK EXAMPLE

Reservoir, Well, Fluid Properties

μ	*(cp)*	0.02	φ_m		0.15
B	*(RCF/SCF)*	1	σ	*(1/ft^2)*	39.47
$c_{t,m}$	*(1/psi)*	1.5×10^{-4}	r_m	*(ft)*	0.5
$c_{t,f}$	*(1/psi)*	5×10^{-4}	f		0.1
h	*(ft)*	30	φ_f		3.94×10^{-5}
L	*(ft)*	5000	$r_{m,1}$	*(ft)*	0.5
q	*(SCF/D)*	1000	$r_{m,2}$	*(ft)*	0.437
k_m	*(md)*	1×10^{-5}	$r_{m,3}$	*(ft)*	0.347

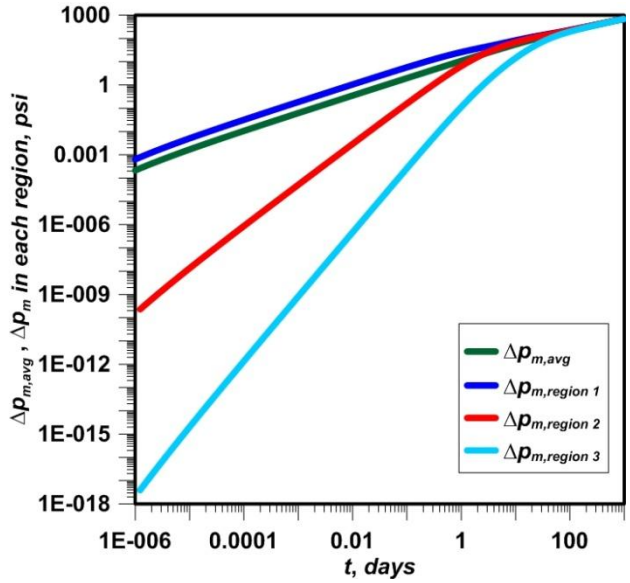

Figure 7.2: Average pressure drop in the spherical matrix and the pressure drops in each region

As shown in **Fig. 7.2**, the pressure drop in region 1, which is the outer and thinner region, follows the average pressure drop profile of whole matrix block. However, the second and third regions require longer times to follow the same line. For example, it requires about 30 days for the third region to reach the matrix average pressure drop.

CHAPTER 8
FIELD APPLICATIONS

In addition to the theoretical examples, in this thesis, I analyzed four field examples from unconventional reservoirs. These four field examples include three long-term production data from one gas and two separate oil wells, and a pressure build-up example from an oil well. The flowing pressure histories for the oil wells were estimated from surface pressure measurements.

8.1 Example 1: Long-Term Production Data From a Horizontal Well in Bakken in Field 1

The first example is a 8794-ft horizontal well in the Middle Bakken formation with open hole completion and single-stage hydraulic fracture in Field 1. The well has been producing for four years. To analyze the long-term production data, I used ***rate normalized pressure*** ($\Delta p/q_o$) vs ***square-root of time*** ($t^{1/2}$) plot. The linear flow equation for uniform matrix blocks (**Eq. 6.21**) can be written in the following form:

$$\frac{\Delta p_f(t)}{q} = \frac{(8.128)\sqrt{24}B\mu}{\sqrt{k_{f,eff}}hL}\left(\frac{1}{(\phi\mu c_t)_{f+m}}\right)^{1/2}\sqrt{t} \qquad [8.1]$$

And the effective permeability is:

$$k_{f,eff} = \left(\frac{8.128B\mu}{m_{linear}hL}\right)^2 \frac{24}{(\phi\mu c_t)_{f+m}} \qquad [8.2]$$

Fig. 8.1 shows the rate normalized pressure data as a function of square-root of time. It is clear that linear flow regime dominates the long term production from the horizontal well in Field 1. The fluid properties are estimated from the PVT analysis and given in **Table 8.1**. I used the typical values of the matrix and fracture compressibilities in Bakken formation. Firstly, we analyzed the linear flow period by assuming the matrix blocks are uniform. Then, we extended our analysis for a triple-matrix example to show the effect of heterogeneity of matrix blocks on the effective permeability estimation.

Production data analyses show that a typical horizontal well in Bakken has an effective producing length which is about 20% of the total length (Kurtoglu, et al., 2012a). Thus, I used the effective producing length as 1760 ft to estimate the effective permeability. From the linear flow analysis for uniform matrix blocks, the ***effective permeability*** was estimated as **3.66×10^{-2} *md***. This calculated

permeability value is relatively high compared to the core measured permeability, which is about 10^{-5} *md*. This enhancement is because of the existent natural fractures.

TABLE 8.1 – DATA FOR BAKKEN FIELD EXAMPLE-1

Reservoir, Well, Fluid Properties

μ	*(cp)*	0.4543	h	*(ft)*	45
B	*(RB/STB)*	1.3669	L	*(ft)*	1760
$c_{t,m}$	*(1/psi)*	$1x10^{-6}$	φ_f		$2x10^{-3}$
$c_{t,f}$	*(1/psi)*	$1x10^{-5}$	φ_m		0.04

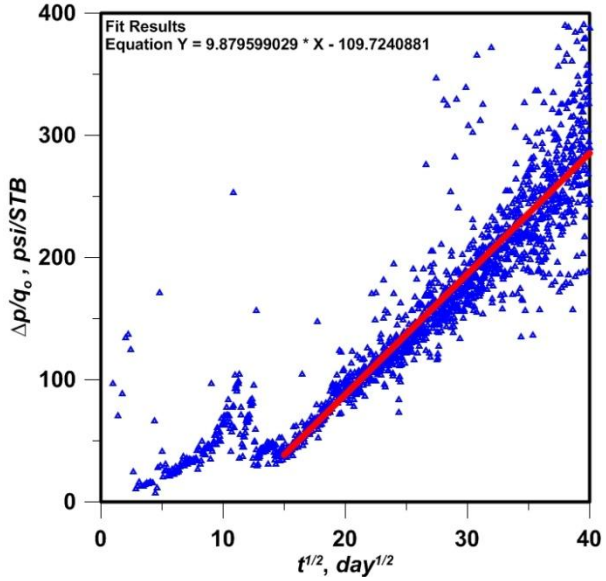

Figure 8.1: Long term production data from a single-stage hydraulically fractured horizontal well in the Bakken in Field 1

Secondly, we estimated the effective formation permeability by assuming the representative elementary volume of this example includes three different matrix blocks. The properties of each matrix block is tabulated below (**Table 8.2**).

TABLE 8.2 – TRIPLE-MATRIX PROPERTIES FOR FIELD EXAMPLE-1

		Matrix Block-1	Matrix Block-2	Matrix Block-3
φ_m		0.04	0.08	0.12
c_{tm}	*(1/psi)*	10^{-6}	10^{-6}	10^{-6}
f		0.3	0.4	0.3

In this case, the compressibilities of the matrix blocks were identical, however, the porosities were different. We used the closed-form solution of linear flow in multiple-matrix setting, **Eq. 6.40**, and estimated the effective permeability as **2.19×10^{-2} *md*** which is 40% less than the uniform matrix case.

8.2 Example 2: Long-Term Production Data From a Horizontal Well in Bakken in Field 2

Example 2 is another horizontal well in the Middle Bakken formation in a different field, Field 2. It is a 20-stage hydraulically fractured horizontal well. When we plot the normalized pressure vs. square-root of time, we again see that linear flow regime dominates long-term production performance (**Fig. 8.2**). The fluid and well data are given in **Table 8.3**.

TABLE 8.3 – DATA FOR BAKKEN FIELD EXAMPLE-2

Reservoir, Well, Fluid Properties

μ	*(cp)*	0.3917	h	*(ft)*	52
B	*(RB/STB)*	1.6147	L	*(ft)*	1920
$c_{t,m}$	*(1/psi)*	2×10^{-6}	φ_f		2×10^{-3}
$c_{t,f}$	*(1/psi)*	1×10^{-5}	φ_m		0.05

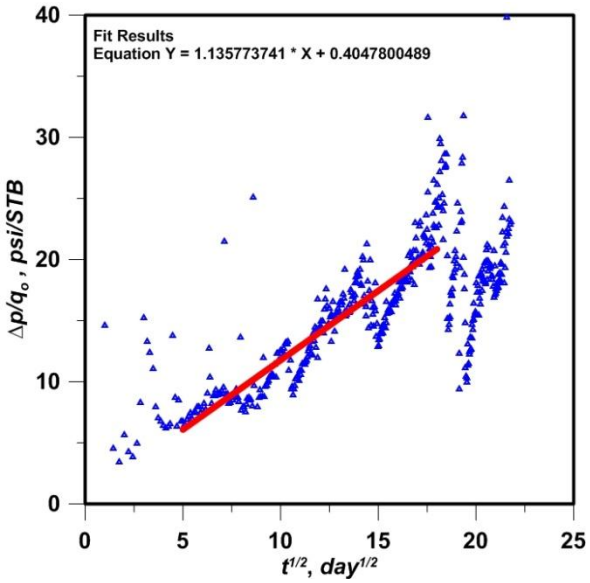

Figure 8.2: Long term production data from a 20-stage hydraulically fractured horizontal well in the Bakken in Field 2

I calculated the ***effective permeability*** as **1.049 *md***, using the uniform matrix solution, **Eq. 8.2**. Because it is a multi-stage hydraulically fractured horizontal well, the calculated effective permeability is higher than the permeability estimated from the first example.

Similar to the field example-1, I generated a theoretical REV containing three different matrix blocks (see **Table 8.4**). In this example, I used a uniform matrix porosity as 0.05. On the other hand, the compressibilities of each matrix block were different: **$2x10^{-6}$ *psi*$^{-1}$**, **$1x10^{-6}$ *psi*$^{-1}$**, **$5x10^{-7}$ *psi*$^{-1}$**. The calculated ***effective permeability*** for this case was **1.799 *md***.

TABLE 8.4 – TRIPLE-MATRIX PROPERTIES FOR FIELD EXAMPLE-2

		Matrix Block-1	Matrix Block-2	Matrix Block-3
φ_m		0.05	0.05	0.05
c_{tm}	*(1/psi)*	$2x10^{-6}$	$1x10^{-6}$	$5x10^{-7}$
f		0.2	0.4	0.4

8.3 Example 3: Long-Term Shale Gas Production Data From a Horizontal Well in Field 3

In addition to two oil well production performance, in this example, I present a long-term gas well production data (**Fig. 8.3**). This production history was obtained from the paper by Nobakht and Mattar (2010). Because the fluid and well data were not provided, I used the data given in **Table 8.5**. To analyze the long-term gas production data, I modified our formulation for the gas flow, as shown below.

Eq. 6.21 can be written in the following form:

$$\frac{\Delta p_f(t)}{q_g \mu_g} = \frac{(8.128)\sqrt{24}B_g}{\sqrt{k_{f,eff}}hL}\left(\frac{1}{(\phi c_t)_{f+m}\mu_g}\right)^{1/2}\sqrt{t} \qquad [8.3]$$

The gas formation volume factor is:

$$B_g = z\frac{p_{sc}}{p}\frac{T}{T_{sc}} \qquad [8.4]$$

The normalized pressure equation for gas flow becomes:

$$\frac{p_i^2 - p_{wf}^2}{q_g \mu_g} = \frac{2(8.128)\sqrt{24}}{5.6146}\frac{\left(z\frac{p_{sc}}{T_{sc}}T\right)}{\sqrt{k_{f,eff}}hL}\left(\frac{1}{(\phi c_t)_{f+m}\mu_g}\right)^{1/2}\sqrt{t} \qquad [8.5]$$

TABLE 8.5 – DATA FOR SHALE GAS FIELD EXAMPLE

Reservoir, Well, Fluid Properties

μ	*(cp)*	0.02	h	*(ft)*	55
z	*(fraction)*	1	L	*(ft)*	4000
$c_{t,m}$	*(1/psi)*	2×10^{-4}	φ_f		1×10^{-3}
$c_{t,f}$	*(1/psi)*	1×10^{-4}	φ_m		0.08

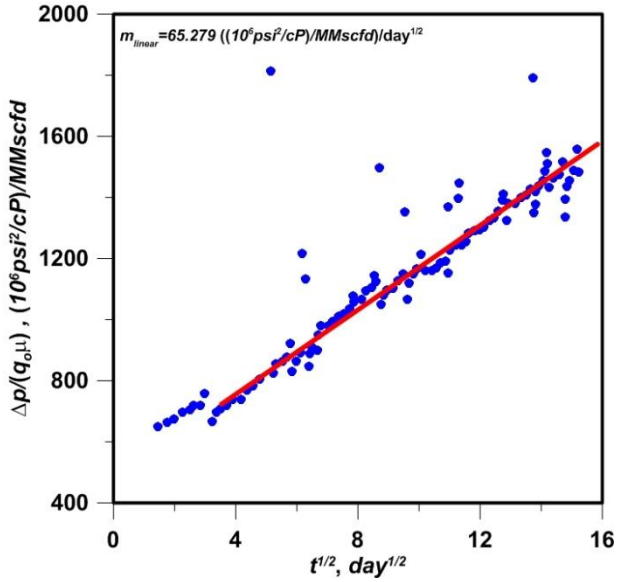

Figure 8.3: A typical long-term shale gas production data (Nobakht and Mattar, 2010)

The effective formation permeability is estimated 9.33×10^{-4} md, which shows the tight nature of shale formations.

8.4 Example 4: Pressure Transient Test Example From a Horizontal Well in Bakken in Field 3

Example-4 is a pressure build-up example from an ***un-stimulated horizontal well*** in the Middle Bakken formation with ***open hole completion*** in Field 4. Ten days initial production was followed by three day shut in period. **Fig. 8.4** presents the pressure and pressure derivative profiles on a log-log plot. As seen in the figure, early time period is masked by the wellbore storage and it is followed by a quarter slope which reflects the bilinear flow regime.

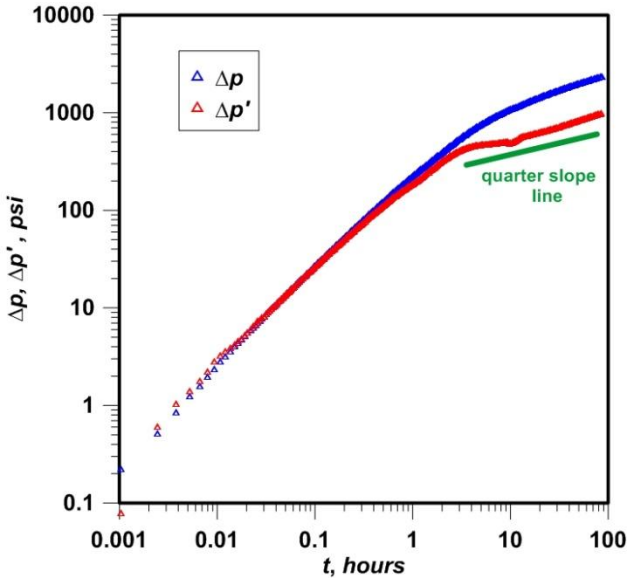

Figure 8.4: Pressure and pressure derivative for field Example 4

To analyze the bilinear flow period, I used the Δp_{ws} vs $t^{1/4}$ plot (see **Fig. 8.5**) and **Eq. 6.17**. The bilinear flow solution requires extra parameters such as matrix permeability and the shape factor. In this analysis, core measured permeability was used as uniform matrix permeability and the typical natural fracture spacing of un-stimulated wells in Bakken was used to calculate the shape factor. Because it is an un-stimulated horizontal well, I used the total length of the well to estimate the effective permeability. The ***effective permeability*** is calculated as **1.28×10^{-4} *md***, based on the data given in **Table 8.6**. When we compare this effective permeability value with the values calculated from Example 1 and Example 2, the bilinear flow permeability of **Fig. 8.4** is the smallest effective permeability, because this test was conducted in an un-stimulated horizontal well.

TABLE 8.6 – DATA FOR BILINEAR FLOW ANALYSIS

Reservoir, Well, Fluid Properties

μ	*(cp)*	0.4883	k_m	*(md)*	3×10^{-5}
B	*(RB/STB)*	1.364	q_{avg}	*(STB/D)*	69
$c_{t,m}$	*(1/psi)*	1×10^{-6}	σ	*(1/ft²)*	0.2
$c_{t,f}$	*(1/psi)*	1×10^{-5}	φ_f		2×10^{-3}
h	*(ft)*	38	φ_m		0.04
L	*(ft)*	9097			

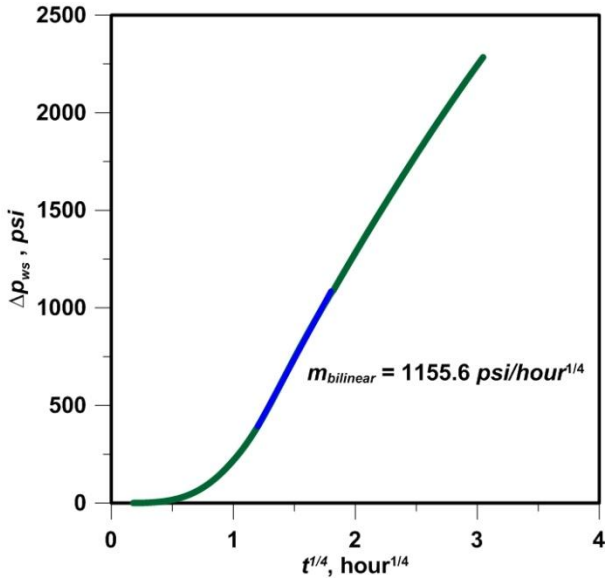

Figure 8.5: Bilinear flow analysis plot

Similar to the linear flow analysis, the permeability can be estimated from the bilinear flow period by considering the heterogeneity of the matrix blocks. In this case, three different matrix blocks having different permeabilities were used. The properties of the matrix blocks and their statistical distribution in the REV are tabulated below. The ***effective permeability*** for this case was calculated as **3.94×10^{-4} *md***.

TABLE 8.7 – TRIPLE-MATRIX PROPERTIES FOR FIELD EXAMPLE-4

	Matrix Block-1	Matrix Block-2	Matrix Block-3
k_m *(md)*	3×10^{-5}	3×10^{-6}	1×10^{-6}
c_{tm} *(1/psi)*	10^{-6}	10^{-6}	10^{-6}
φ_m	0.04	0.04	0.04
σ *(1/ft^2)*	0.2	0.2	0.2
f	0.2	0.4	0.4

CHAPTER 9
DISCUSSION, CONCLUSIONS AND RECOMMENDATIONS

In this thesis, I have presented a mathematical formulation to more accurately capture the flow contributions from matrix blocks of various size, permeability, and porosity in dual-porosity fractured reservoirs -- specially in unconventional reservoirs. I chose both the pseudo-steady state and the unsteady state (USS) fluid transfer models, and obtained solutions for the unsteady state transfer functions for matrix blocks having different shapes and properties. Also, I reported closed-form solutions for single- and multiple-matrix problems (linear and bilinear flow regimes) to be used in pressure transient test analysis of conventional and unconventional reservoirs. In addition to the single-phase flow solutions, a known water-oil flow transfer function was used for matching experimental oil recovery results and as a basis for modeling the ***counter-current flow*** from the matrix in field operations.

The multiple-matrix model presented in this thesis captures the effect of matrix size and heterogeneity of the matrix blocks. Heterogeneity includes permeability, porosity, geometry, and shape factor.

The closed-form solutions for multiple-matrix model presented in Chapter 5 can be used in the pressure and rate transient analyses of linear and bilinear flow regimes in fractured reservoirs.

The USS transfer function solution used in pressure transient analysis indicates that the classical pseudo-steady-state (PSS) V-shape characteristic of the pressure derivative plot for dual-porosity reservoirs is unrealistic, especially for unconventional reservoirs. This conclusion is consistent with observations and results from well tests in the field. The only situation that leads the V-shape character in the derivative plot is large permeability contrast between two communicating layers (Al-Ajmi, et al., 2008).

The most notable simulation result is that the matrix contribution to flow is very slow in typical unconventional reservoirs. The matrix permeability and the matrix size are the key factors in determining the contribution of matrix block to the overall production.

Finally, because of the difficulties in measuring the relative permeability in unconventional tight matrix, the water-oil formulation presented in this study can be used as a substitute to predict matrix drainage and reservoir performance. A comprehensive presentation of this topic is postponed to a future PhD thesis.

The multiple-matrix formulation presented in this thesis can be extended to multi-phase, multi-component flow problems. For instance, in addition to size and shape heterogeneities, different relative permeability and capillary pressure data can be assigned to different matrix blocks for multi-phase flow problems. Also, multiple-matrix model can be used to capture the heterogeneity based on pore-size distribution and PVT data of the matrix. For example, each matrix block can have a different average pore size. Accordingly, different phase behavior can be assigned to each matrix block to reflect the confined pore space heterogeneity.

LIST OF SYMBOLS

A_m : *surface area of matrix block,* L^2 *(*ft^2*)*

B : *formation volume factor,* L^3/L^3 *(RB/STB or RCF/SCF)*

B_g : *gas formation volume factor,* L^3/L^3 *(RCF/SCF)*

$c_{t,\,m}$: *total matrix compressibility,* L^2F^{-1} *(1/psi)*

$c_{t,\,f}$: *total fracture compressibility,* L^2F^{-1} *(1/psi)*

f : *volume fraction of each matrix block in REV, fraction*

h : *formation thickness, L (ft)*

$k_{f,\,eff}$: *effective fracture permeability (fracture porosity x fracture permeability),* L^2 *(md)*

k_m : *matrix permeability,* L^2 *(md)*

L : *horizontal well length, L (ft)*

L_z : *thickness of a slab matrix block, L (ft)*

$L_{x,y,z}$: *dimensions of a cuboid matrix block, L (ft)*

$m_{intermediate}$: *slope of bilinear flow,* $FL^{-2}T^{-1/4}$ *(*$psi/hr^{1/4}$*)*

m_{late} : *slope of linear flow,* $FL^{-2}T^{-1/2}$ *(*$psi/hr^{1/2}$*)*

N_b : *number of matrix block in REV or CV*

μ : *oil viscosity,* W/LT *(cp)*

μ_g : *gas viscosity,* W/LT *(cp)*

φ_m : *matrix porosity, %*

φ_f : *fracture porosity, %*

q : *oil production rate,* L^3T^{-1} *(*ft^3*/D for Eq. 16 through 19, BBL/D for Eq. 30 through 54)*

q_g : *gas production rate,* L^3T^{-1} *(SCF/D)*

q_m : *matrix counter-current flow rate,* L^3T^{-1} *(RCF/D)*

$q_{u,m}$: *flowrate caused by a unitary pressure loss at the matrix surface,* $L^5F^{-1}T^{-1}$ *(*$ft^3psi^{-1}D^{-1}$*)*

$\hat{q}_{u,m}$: *flowrate caused by a unitary pressure loss at the matrix surface by unit rock volume,* $L^2F^{-1}T^{-1}$ *(*$psi^{-1}D^{-1}$*)*

p_{Df} : *dimensionless pressure drop in the fracture*

p_i : *initial reservoir pressure,* FL^{-2} *(psi)*

p_m^o : *matrix initial pressure,* FL^{-2} *(psi)*

p_m : *matrix pressure at any time t,* FL^{-2} *(psi)*

p_{sc} : *standard condition pressure,* FL^{-2} *(psi)*

p_{wf} : *well flowing pressure,* FL^{-2} *(psi)*

R : *oil volume recovery per unit rock volume at any time, t,* L^3/L^3

R_∞ : *maximum oil volume recovery per unit rock volume at infinity time,* L^3/L^3

r : *Spherical r-coordinate, L (ft)*

r_m : *radius of spherical matrix block, L (ft)*

V_m : *matrix control volume,* L^3 *(ft^3)*

s : *The Laplace transform variable*

S_{wf} : *water saturation in the fracture, fraction*

S_{wm} : *water saturation in the matrix, fraction*

S_{orm} : *irreducible oil saturation in the matrix, fraction*

S_{wrm} : *irreducible water saturation in the matrix, fraction*

t : *time, T (day for Eq. 1 through 21 and Eq. 40 through 58, hour for Eq. 30 through 39)*

T : *reservoir temperature, (°R)*

T_{sc} : *standard condition temperature, (°R)*

$u_{t,f}$: *water injection velocity,* L/T *(ft/day)*

x : *Cartesian x-coordinate perpendicular to the horizontal well, L (ft)*

x_D : *dimensionless distance to the production well in Cartesian x-coordinate*

z : *gas deviation factor*

σ : *shape factor,* $1/L^2$ *(1/ft^2)*

ω : *storativity ratio of fracture to the total system*

λ : *interporosity flow parameter*

$\tilde{\lambda}$: *exponential decline parameter, T^{-1} (1/D)*

τ : *unsteady-state transfer function, T^{-1} (1/D)*

η_m : *matrix diffusivity coefficient,* L^2/T *(ft^2/day)*

$\Delta p'$: *pressure logarithmic derivative,* FL^{-2} *(psi)*

Δp_m : *unitary step pressure change in a matrix block,* FL^{-2} *(psi)*

Δp_f : *pressure change in fracture,* FL^{-2} *(psi)*

Δp_{wf} : *well flowing pressure change,* FL^{-2} *(psi)*

Δp_{ws} : *well static pressure change,* FL^{-2} *(psi)*

REFERENCES CITED

Al-Ajimi, N. M., Kazemi, H., Ozkan, E. 2008. Estimation of storativity ratio in a layered reservoir with crossflow. *SPE Reservoir Evolution & Engineering* (April 2008), 267-279.

Alamdari, B. B., Kiani, M., Kazemi, H. 2012. Experimental and numerical simulation of surfactant-assisted oil recovery in tight fractured carbonate reservoir cores. Paper SPE 153902 presented at the Eighteenth SPE Improved Oil Recovery Symposium, Tulsa, OK, USA, 14 – 18 April 2012.

Alharthy, N., Kobaisi, M. A., Torcuk, M. A., Kazemi, H., Graves, R. 2012. Physics and modeling of gas flow in shale reservoirs. Paper SPE 161893 presented at the Abu Dhabi International Petroleum Exhibition & Conference, Abu Dhabi, UAE, 11 – 14 November 2012.

Barenblatt, G. I., Zeltov, Y. P., and Kochina, I. 1960. Basic concepts in the theory of seepage of homogeneous liquids in fissured rocks. *PMM* (*Journal of Soviet Applied Mathematics and Mechanics*), 24(5): 1286-1303.

Carslaw, H.S. and Jaeger, J.C. 1959. Conduction of heat in solids. 2nd ed., Oxford U. Press, New York.

de Swaan-O, A. 1976. Analytic solutions for determining naturally fractured reservoir properties by well testing. *SPE Journal* (June 1976) *117-122; Trans.,* AIME 261.

de Swaan-O, A. 1978. Theory of waterflooding in fractured reservoirs. *SPE Journal* (April 1978) 117-22, *Trans.* AIME 265.

Du, K. and Stewart, G., 1992. Transient pressure response of horizontal wells in layered and naturally fractured reservoirs with dual porosity behavior. Paper SPE 24682 presented at 1992 SPE Annual Technical Conference and Exhibition, Washington, District of Columbia, USA.

Du, K. and Stewart, G., 1995. Bilinear flow regime occurring in horizontal wells and other geological models. Paper SPE 29960 presented at 1995 SPE International Meeting on Petroleum Engineering, Beijing, PR China.

Kazemi, H. 1969. Pressure transient analysis of naturally fractured reservoirs with uniform fracture distribution. *SPE Journal*, 9(4):451-462.

Kazemi, H., Gilman, J. R., Elsharkawy, A. M. 1992. Analytical and numerical solution of oil recovery from fractured reservoirs with empirical transfer functions. *SPE Reservoir Engineering* (May 1992), 219-227.

Kazemi, H. and Gilman, J. R. 1993. Multiphase flow in fractured petroleum reservoirs. Flow and Contaminant Transport in Fractured Rocks, pages 267-323.

Kurtoglu, B., Torcuk, M. A., Kazemi, H. 2012a. Pressure transient analyses of short and long duration well tests in unconventional reservoirs. Paper SPE 162473 presented at the Canadian Unconventional Resources Conference, Calgary, Alberta, Canada, 30 October-1 November 2012.

Kurtoglu, B. and Kazemi, H., 2012b. Evaluation of Bakken Performance Using Coreflooding, Well Testing, and Reservoir Simulation. Paper SPE 155655 presented at 2012 SPE Annual Technical Conference and Exhibition, San Antonio, Texas, USA.

Najurieta, H. L., 1980. A theory for pressure transient analysis in naturally fractured reservoirs. *Journal of Petroleum Technology*, (July 1980) 1241-50.

Nobakht, M. and Mattar, L. 2010. Analyzing production data from unconventional gas reservoirs with linear flow and apparent skin. Paper SPE 137454 presented at 2010 SPE Canadian Unconventional Resources & International Petroluem Conference, Calgary, Alberta, Canada.

Pruess, K. and Narasimhan, T. H. 1985. A practical method for modeling fluid and heat flow in fractured porous media. *Soc. Pet. Eng. J.*, 25, 14-26, 1985.

Stehfest, H., 1970. Numerical Inversion of Laplace Transforms. Communications of the ACM, D-5 13, No. 1, pg: 47-49.

Torcuk, M. A., Kurtoglu, B., Alharthy, N. and Kazemi, H. 2013. Analytical and numerical solutions for multiple-matrix in fractured reservoirs, application to conventional and unconventional reservoirs. Paper SPE 164528 presented at 2013 SPE Unconventional Resources Conference, The Woodlands, Texas, USA.

van Everdingen, A. and Hurst, W. 1949. The application of the Laplace transformation to flow problems in reservoirs. Trans., AIME, 186:305-324.

Warren, J. E. and Root, P. J. 1963. The behavior of naturally fractured reservoirs. SPE Journal, 3(3):245-255.

APPENDIX A

DERIVATION OF UNSTEADY-STATE TRANSFER FUNCTIONS

The USS transfer function for a spherical matrix block is presented by **Eqs. 3.5, 3.6** and **3.7**. I differentiate **Eq. 3.7** to get the pressure gradient at surface of the spherical matrix block for use in **Eq. 3.6**.

$$\left(\frac{\partial p_m}{\partial r}\right)_{r_m} = -\frac{2}{r_m}\sum_{n=1}^{\infty}\exp\left(\frac{-\eta_m n^2\pi^2 t}{r_m^2}\right) \qquad [A1]$$

Plugging **Eq. A1** into **Eq. 3.6**, and dividing by the volume of the spherical matrix, I get:

$$\hat{q}_{u,m}(x,t) = 0.006328\frac{k_m A_m}{V_m \mu}\frac{2}{r_m}\left[\sum_{n=1}^{\infty}\exp\left(\frac{-\eta_m n^2\pi^2 t}{r_m^2}\right)\right] \qquad [A2]$$

For a sphere, the surface to volume ratio, A_m/V_m , is $3/r_m$. Thus **Eq. A2** can be written in the following form:

$$\hat{q}_{u,m}(x,t) = 0.006328\frac{k_m}{\mu}\left(\frac{\pi^2}{r_m^2}\right)\frac{6}{\pi^2}\left[\sum_{n=1}^{\infty}\exp\left(\frac{-\eta_m n^2\pi^2 t}{r_m^2}\right)\right] \qquad [A3]$$

The quantity π^2/r_m^2 is called the ***shape factor*** for a spherical matrix block. Thus, the USS transfer function, **Eq. 3.5**, becomes:

$$\tau(x,t) = 0.006328\frac{k_m}{\mu}\sigma\frac{6}{\pi^2}\int_0^t \frac{\partial \Delta p_f(x,t)}{\partial \xi}\left[\sum_{n=1}^{\infty}\exp\left(-\eta_m n^2\sigma(t-\xi)\right)\right]d\xi \qquad [A4]$$

Similarly, the USS transfer function for a slab matrix can be derived, as shown in **Eq. 3.13**.

The derivation of the USS transfer function for a cuboid matrix block follows similar steps as in the spherical case. However, this derivation involves integration over six faces of the cuboid. I start with the unit step function in a cuboid to derive the USS transfer function for a cuboid matrix block. The unit step function for a cuboid matrix block is (Carslaw and Jaeger, 1959):

$$\Delta p\left(x,t,\hat{x},\hat{y},\hat{z}\right)=1+\left\{\begin{array}{l}\dfrac{64}{\pi^3}\displaystyle\sum_{l=0}^{\infty}\sum_{m=0}^{\infty}\sum_{n=0}^{\infty}\dfrac{(-1)^l(-1)^m(-1)^n}{(2l+1)(2m+1)(2n+1)}\\ \cos\left[\dfrac{(2l+1)\pi\hat{x}}{L_x}\right]\cos\left[\dfrac{(2m+1)\pi\hat{y}}{L_y}\right]\cos\left[\dfrac{(2n+1)\pi\hat{z}}{L_z}\right]\\ \exp\left[-\eta_m\pi^2\left(\dfrac{(2l+1)^2}{L_x^2}+\dfrac{(2m+1)^2}{L_y^2}+\dfrac{(2n+1)^2}{L_z^2}\right)t\right]\end{array}\right\} \quad [A5]$$

Where: $\Delta p\left(x,t,\hat{x},\hat{y},\hat{z}\right)=p_m^o-p_m\left(x,t,\hat{x},\hat{y},\hat{z}\right)$ [A6]

The flow rate from the matrix into the fracture along the y-z plane of the matrix block at $\hat{x}=\dfrac{L_x}{2}$ is:

$$q_{\hat{x}}\Big|_{\hat{x}=\frac{L_x}{2}}=-0.006328\frac{k_m}{\mu}\int_{-\frac{L_y}{2}}^{\frac{L_y}{2}}\int_{-\frac{L_z}{2}}^{\frac{L_z}{2}}\frac{\partial p}{\partial\hat{x}}\Big|_{\hat{x}=\frac{L_x}{2}}d\hat{y}d\hat{z} \quad [A7]$$

The pressure gradient at the y-z plane of the matrix block at $\hat{x}=\dfrac{L_x}{2}$ is calculated by differentiating **Eq. A5** as shown:

$$\frac{\partial p}{\partial\hat{x}}\Big|_{\hat{x}=\frac{L_x}{2}}=-\frac{64}{\pi^3}\left\{\begin{array}{l}\displaystyle\sum_{l=0}^{\infty}\sum_{m=0}^{\infty}\sum_{n=0}^{\infty}\frac{(-1)^m(-1)^n}{(2m+1)(2n+1)}\left\{\frac{1}{(2l+1)}\frac{(2l+1)\pi}{L_x}(-1)^l\sin\left(\frac{(2l+1)\pi}{2}\right)\right.\\ \cos\left[\dfrac{(2m+1)\pi\hat{y}}{L_y}\right]\cos\left[\dfrac{(2n+1)\pi\hat{z}}{L_z}\right]\\ \left.\exp\left[-\eta_m\pi^2\left(\dfrac{(2l+1)^2}{L_x^2}+\dfrac{(2m+1)^2}{L_y^2}+\dfrac{(2n+1)^2}{L_z^2}\right)t\right]\right\}\end{array}\right\} \quad [A8]$$

The product of $(-1)^l$ *and* $\sin\left(\dfrac{(2l+1)\pi}{2}\right)$ is always +1, thus **Eq. A8** can be written as:

$$\left.\frac{\partial p}{\partial \hat{x}}\right|_{\hat{x}=\frac{L_x}{2}} = -\frac{64}{\pi^3}\sum_{l=0}^{\infty}\sum_{m=0}^{\infty}\sum_{n=0}^{\infty}\frac{(-1)^m(-1)^n}{(2m+1)(2n+1)}\left\{\begin{array}{l}\frac{\pi}{L_x}\cos\left[\frac{(2m+1)\pi\hat{y}}{L_y}\right]\cos\left[\frac{(2n+1)\pi\hat{z}}{L_z}\right] \\ \exp\left[-\eta_m\pi^2\left(\frac{(2l+1)^2}{L_x^2}+\frac{(2m+1)^2}{L_y^2}+\frac{(2n+1)^2}{L_z^2}\right)t\right]\end{array}\right\} \quad \text{[A9]}$$

Plugging **Eq. A9** into the flow rate equation, **Eq. A7**, gives:

$$q_{\hat{x}}\big|_{\hat{x}=\frac{L_x}{2}} = 0.006328\frac{k_m}{\mu}\left\{\begin{array}{l}\frac{64}{\pi^3}\sum_{l=0}^{\infty}\sum_{m=0}^{\infty}\sum_{n=0}^{\infty}\frac{(-1)^m(-1)^n}{(2m+1)(2n+1)} \\ \left(\frac{\pi}{L_x}\left[\int_{-\frac{L_y}{2}}^{\frac{L_y}{2}}\cos\left(\frac{(2m+1)\pi\hat{y}}{L_y}\right)d\hat{y}\int_{-\frac{L_z}{2}}^{\frac{L_z}{2}}\cos\left(\frac{(2n+1)\pi\hat{z}}{L_z}\right)d\hat{z}\right]\right) \\ \exp\left[-\eta_m\pi^2\left(\frac{(2l+1)^2}{L_x^2}+\frac{(2m+1)^2}{L_y^2}+\frac{(2n+1)^2}{L_z^2}\right)t\right]\end{array}\right\} \quad \text{[A10]}$$

And

$$\int_{-\frac{L_y}{2}}^{\frac{L_y}{2}}\cos\left(\frac{(2m+1)\pi\hat{y}}{L_y}\right)d\hat{y} = \frac{L_y}{(2m+1)\pi}\left[\sin\left(\frac{(2m+1)\pi}{2}\right)-\sin\left(\frac{-(2m+1)\pi}{2}\right)\right] \quad \text{[A11]}$$

$$\int_{-\frac{L_z}{2}}^{\frac{L_z}{2}}\cos\left(\frac{(2n+1)\pi\hat{z}}{L_y}\right)d\hat{z} = \frac{L_z}{(2n+1)\pi}\left[\sin\left(\frac{(2n+1)\pi}{2}\right)-\sin\left(\frac{-(2n+1)\pi}{2}\right)\right] \quad \text{[A12]}$$

The product of $(-1)^m$ *and* $\left[\sin\left(\frac{(2m+1)\pi}{2}\right)-\sin\left(\frac{-(2m+1)\pi}{2}\right)\right]$, and the product of $(-1)^n$ and $\left[\sin\left(\frac{(2n+1)\pi}{2}\right)-\sin\left(\frac{-(2n+1)\pi}{2}\right)\right]$ are always +2, thus the flow rate equation becomes:

$$q_{\hat{x}}\big|_{\hat{x}=\frac{L_x}{2}} = 0.006328\frac{k_m}{\mu}\left\{\begin{array}{l}\frac{64}{\pi^3}\sum_{l=0}^{\infty}\sum_{m=0}^{\infty}\sum_{n=0}^{\infty}\frac{1}{(2m+1)^2(2n+1)^2}\left(\frac{4}{\pi}\right)\left(\frac{L_yL_z}{L_x}\right) \\ \exp\left[-\eta_m\pi^2\left(\frac{(2l+1)^2}{L_x^2}+\frac{(2m+1)^2}{L_y^2}+\frac{(2n+1)^2}{L_z^2}\right)t\right]\end{array}\right\} \quad \text{[A13]}$$

I also note that the flow rate from the matrix into the fracture along the surface $\hat{x}=-L_x/2$, $q_{\hat{x}}\big|_{\hat{x}=-L_x/2}$, is the same as the flow rate from the matrix into the fracture along the surface $\hat{x}=L_x/2$. Therefore, the flow rate per unit rock volume along the surface $\hat{x}=L_x/2$ is:

$$\hat{q}_{\hat{x}}\big|_{\hat{x}=\frac{L_x}{2}}=\frac{q_{\hat{x}}\big|_{\hat{x}=\frac{L_x}{2}}}{L_xL_yL_z}=0.006328\frac{k_m}{\mu}\left\{\begin{array}{l}\left(\frac{4}{L_x^2}\right)\left(\frac{1}{\pi}\right)\left(\frac{64}{\pi^3}\right)\sum_{l=0}^{\infty}\sum_{m=0}^{\infty}\sum_{n=0}^{\infty}\frac{1}{(2m+1)^2(2n+1)^2}\\ \exp\left[-\eta_m\pi^2\left(\frac{(2l+1)^2}{L_x^2}+\frac{(2m+1)^2}{L_y^2}+\frac{(2n+1)^2}{L_z^2}\right)t\right]\end{array}\right\} \quad [A14]$$

Then, the total flow rate per unit rock volume along the two surfaces at $\hat{x}=\pm\frac{L_x}{2}$ is:

$$\hat{q}_{\hat{x}}\big|_{\hat{x}=\frac{L_x}{2}}+\hat{q}_{\hat{x}}\big|_{\hat{x}=-\frac{L_x}{2}}=0.006328\frac{k_m}{\mu}\left\{\begin{array}{l}\left(\frac{\pi^2}{L_x^2}\right)\left(\frac{512}{\pi^6}\right)\sum_{l=0}^{\infty}\sum_{m=0}^{\infty}\sum_{n=0}^{\infty}\frac{1}{(2m+1)^2(2n+1)^2}\\ \exp\left[-\eta_m\pi^2\left(\frac{(2l+1)^2}{L_x^2}+\frac{(2m+1)^2}{L_y^2}+\frac{(2n+1)^2}{L_z^2}\right)t\right]\end{array}\right\} \quad [A15]$$

The total flow rates along the other four surfaces can be obtained, similarly. Adding all the flow rates coming from 6 surfaces of a cuboid matrix block, I get:

$$\hat{q}_{u,m,total}=0.006328\frac{k_m}{\mu}\left\{\begin{array}{l}\left(\frac{512}{\pi^6}\right)\sum_{l=0}^{\infty}\sum_{m=0}^{\infty}\sum_{n=0}^{\infty}\frac{(2l+1)^2\frac{\pi^2}{L_x^2}+(2n+1)^2\frac{\pi^2}{L_y^2}+(2m+1)^2\frac{\pi^2}{L_z^2}}{(2l+1)^2(2n+1)^2(2m+1)^2}\\ \exp\left[-\eta_m\pi^2\left(\frac{(2l+1)^2}{L_x^2}+\frac{(2m+1)^2}{L_y^2}+\frac{(2n+1)^2}{L_z^2}\right)t\right]\end{array}\right\} \quad [A16]$$

Thus, the USS transfer function for a cuboid matrix block becomes:

$$\tau(x,t) = 0.006328 \frac{k_m}{\mu} \frac{512}{\pi^6} \int_0^t \frac{\partial \Delta p_f(x,t)}{\partial \xi} \left[\sum_{l=0}^{\infty} \sum_{m=0}^{\infty} \sum_{n=0}^{\infty} \left(\frac{\pi^2 \left(\frac{(2l+1)^2}{L_x^2} + \frac{(2m+1)^2}{L_y^2} + \frac{(2n+1)^2}{L_z^2} \right)}{(2l+1)^2 (2m+1)^2 (2n+1)^2} \right) \right] \exp\left[-\eta_m \pi^2 \left(\frac{(2l+1)^2}{L_x^2} + \frac{(2m+1)^2}{L_y^2} + \frac{(2n+1)^2}{L_z^2} \right) (t-\xi) \right] d\xi \quad \text{[A17]}$$

APPENDIX B

DERIVATION OF THE LAPLACE DOMAIN SOLUTIONS

B.1 Laplace Domain Solutions for Uniform Spherical Matrix Blocks

The dual-porosity pressure diffusivity equation for 1-D linear flow is:

$$\left(0.006328\frac{k_{f,eff}}{\mu}\right)\frac{\partial^2 \Delta p_f(x,t)}{\partial x^2} - \tau = \left(\phi c_t\right)_f \frac{\partial \Delta p_f(x,t)}{\partial t} \qquad [B1]$$

Where:

$$\Delta p_f = p^o - p_f \qquad [B2]$$

The unsteady-state transfer function for a spherical matrix block is:

$$\tau(x,t) = 0.006328\frac{k_m}{\mu}\sigma\frac{6}{\pi^2}\int_0^t \frac{\partial \Delta p_f(x,t)}{\partial \xi}\left[\sum_{n=1}^{\infty}\exp\left(\frac{-\eta_m n^2\pi^2\left(t-\xi\right)}{r_m^2}\right)\right]d\xi \qquad [B3]$$

Applying the Laplace transform to the transfer function, **Eq. B3**, gives:

$$\bar{\tau}(x,s) = 0.006328\frac{k_m}{\mu}\sigma\frac{6}{\pi^2}s\Delta\bar{p}_f(x,s)\sum_{n=1}^{\infty}\frac{1}{s+\sigma\eta_m n^2} \qquad [B4]$$

The diffusivity equation, **Eq. B1**, in the Laplace domain is:

$$\left(0.006328\frac{k_{f,eff}}{\mu}\right)\frac{\partial^2 \Delta\bar{p}_f(x,s)}{\partial x^2} - \bar{\tau} = \left(\phi c_t\right)_f s\Delta\bar{p}_f(x,s) \qquad [B5]$$

Upon substitution of **Eq. B4** in **Eq. B5**, one obtains:

$$\frac{\partial^2 \Delta\bar{p}_f(x,s)}{\partial x^2} = s\left[\frac{\left(\phi\mu c_t\right)_f}{0.006328k_{f,eff}} + \frac{k_m}{k_{f,eff}}\sigma\frac{6}{\pi^2}\sum_{n=1}^{\infty}\frac{1}{s+\sigma\eta_m n^2}\right]\Delta\bar{p}_f(x,s) \qquad [B6]$$

I simplify **Eq. B6** by defining the following function:

$$g(s) = s\left[\frac{\left(\phi\mu c_t\right)_f}{0.006328k_{f,eff}} + \frac{k_m}{k_{f,eff}}\sigma\frac{6}{\pi^2}\sum_{n=1}^{\infty}\frac{1}{s+\sigma\eta_m n^2}\right] \qquad [B7]$$

Thus, the diffusivity equation in the Laplace domain becomes:

$$\frac{\partial^2 \Delta\bar{p}_f(x,s)}{\partial x^2} - g(s)\Delta\bar{p}_f(x,s) = 0 \qquad [B8]$$

This is a homogeneous differential equation with the following solution:

$$\Delta\bar{p}_f(x) = A\exp\left(-\sqrt{g(s)}\,x\right) + B\exp\left(+\sqrt{g(s)}\,x\right) \qquad [B9]$$

For an infinitely large reservoir, $\Delta\bar{p}_f$ is zero when x goes to infinity:

$$\lim_{x\to\infty}\Delta\bar{p}_f(x,s) = A\lim_{x\to\infty}\exp\left(-\sqrt{g(s)}\,x\right) + B\lim_{x\to\infty}\exp\left(+\sqrt{g(s)}\,x\right) = 0 \qquad [B10]$$

However,

$$\lim_{x\to\infty}\exp\left(-\sqrt{g(s)}\,x\right) = 0 \qquad [B11]$$

$$\lim_{x\to\infty}\exp\left(+\sqrt{g(s)}\,x\right) = \infty \qquad [B12]$$

Thus, *B=0* should satisfy the boundary condition given by Eq. 22, and, therefore, Eq. 19 becomes:

$$\Delta\bar{p}_f(x,s) = A\exp\left(-\sqrt{g(s)}\,x\right) \qquad [B13]$$

Now, I need another boundary condition to determine coefficient *A*. By using Darcy's law, I can write the inner boundary condition as following:

$$qB = -(0.006328)\frac{k_{f,eff}}{\mu}hL\left.\frac{\partial\Delta p_f}{\partial x}\right|_{x=0} \qquad [B14]$$

Or,

$$\left.\frac{\partial\Delta p_f}{\partial x}\right|_{x=0} = \frac{-qB\mu}{0.006328\,k_{f,eff}\,hL} \qquad [B15]$$

Applying the Laplace transform to the above boundary condition, I get:

$$\left.\frac{\partial\Delta\bar{p}_f}{\partial x}\right|_{x=0} = \frac{1}{s}\frac{-qB\mu}{0.006328\,k_{f,eff}\,hL} \qquad [B16]$$

Using **Eq. B13**, I obtain:

$$\frac{\partial \Delta \bar{p}_f(x,s)}{\partial x} = -A\sqrt{g(s)}\exp\left(-\sqrt{g(s)}\,x\right) \quad \text{and} \quad \left.\frac{\partial \Delta \bar{p}_f(x,s)}{\partial x}\right|_{x=0} = -A\sqrt{g(s)} \qquad \text{[B17]}$$

Now, I can determine the coefficient *A* from the **Eq. B16** and **B17**:

$$\left.\frac{\partial \Delta \bar{p}_f(x,s)}{\partial x}\right|_{x=0} = -A\sqrt{g(s)} = \frac{1}{s}\frac{-qB\mu}{0.006328 k_{f,eff} hL} \Rightarrow A = \frac{1}{s\sqrt{g(s)}}\frac{qB\mu}{0.006328 k_{f,eff} hL} \qquad \text{[B18]}$$

And, the fracture pressure solution in the Laplace domain for the constant terminal rate case becomes:

$$\Delta \bar{p}_f(x,s) = \frac{1}{s\sqrt{g(s)}}\frac{qB\mu}{0.006328 k_{f,eff} hL}\exp\left(-\sqrt{g(s)}\,x\right) \qquad \text{[B19]}$$

And, for *x=0*, the wellbore pressure solution:

$$\Delta \bar{p}_f(0,s) = \frac{1}{s\sqrt{g(s)}}\frac{qB\mu}{0.006328 k_{f,eff} hL} \qquad \text{[B20]}$$

Where:

$$g(s) = s\left[\frac{(\phi\mu c_t)_f}{0.006328 k_{f,eff}} + \frac{k_m}{k_{f,eff}}\sigma\frac{6}{\pi^2}\sum_{n=1}^{\infty}\frac{1}{s+\sigma\eta_m n^2}\right] \qquad \text{[B21]}$$

To get the constant terminal pressure case solution, I should start from the **Eq. B13**.

$$\Delta \bar{p}_f(x,s) = A\exp\left(-\sqrt{g(s)}\,x\right) \qquad \text{[B22]}$$

Now, I don't have the constant rate inner boundary condition, the new inner boundary condition is constant Δp_f at x=0. This boundary condition in the Laplace domain can be written as following:

$$\Delta \bar{p}_f\big|_{x=0} = \frac{\Delta p_f\big|_{x=0}}{s} \qquad \text{[B23]}$$

We can determine the coefficient A from the **Eq. B23**:

$$\Delta\bar{p}_f\left(x=0,s\right)=\frac{\Delta p_f\big|_{x=0}}{s},\quad A\exp\left(-\sqrt{g\left(s\right)}0\right)=\frac{\Delta p_f\big|_{x=0}}{s},\quad A=\frac{\Delta p_f\big|_{x=0}}{s} \tag{B24}$$

And the constant terminal pressure case solution for any x becomes:

$$\Delta\bar{p}_f\left(x,s\right)=\frac{\Delta p_f\big|_{x=0}}{s}\exp\left(-\sqrt{g\left(s\right)}x\right) \tag{B25}$$

The flow rate can be calculated from the following equation:

$$qB=-\left(0.006328\right)\frac{k_{f,eff}}{\mu}hL\left.\frac{\partial\Delta p_f}{\partial x}\right|_{x=0} \tag{B26}$$

Taking the Laplace transform of **Eq. B26** gives:

$$\bar{q}B=-\left(0.006328\right)\frac{k_{f,eff}}{\mu}hL\left.\frac{\partial\Delta\bar{p}_f}{\partial x}\right|_{x=0} \tag{B27}$$

And

$$\left.\frac{\partial\Delta\bar{p}_f}{\partial x}\right|_{x=0}=\frac{\Delta p_f\big|_{x=0}}{s}\left(-\sqrt{g\left(s\right)}\right) \tag{B28}$$

Thus, the flow rate equation in the Laplace domain, **Eq. B27**, becomes:

$$\bar{q}B=\left(0.006328\right)\frac{k_{f,eff}}{\mu}hL\,\Delta p_f\big|_{x=0}\left(\frac{\sqrt{g\left(s\right)}}{s}\right) \tag{B29}$$

I can also determine the matrix volumetric average pressures after calculating the fracture pressures. To get the matrix volumetric average pressure solution in Laplace domain, I start with the transfer function equation in Laplace domain, **Eq. B4**:

$$\bar{\tau}(x,s)=0.006328\frac{k_m}{\mu}\sigma\frac{6}{\pi^2}s\Delta\bar{p}_f\left(x,s\right)\sum_{n=1}^{\infty}\frac{1}{s+\sigma\eta_m n^2} \tag{B30}$$

I also know the relationship between the transfer function and matrix pressure in real time domain:

$$\tau(x,t)=(\phi c_t)_m \frac{\partial \Delta\hat{p}_m(x,t)}{\partial t} \quad [B31]$$

Where $\Delta\hat{p}_m$ is the matrix volumetric average pressure drop. Taking the Laplace transform of **Eq. B31**, we get:

$$\bar{\tau}(x,s)=(\phi c_t)_m s\Delta\bar{\hat{p}}_m(x,s) \quad [B32]$$

Where $\Delta\bar{\hat{p}}_m$ is the matrix volumetric average pressure drop in the Laplace domain. Substituting **Eq. B30** into **Eq. B32**, we obtain:

$$(0.006328)\frac{k_m}{\mu}\sigma\frac{6}{\pi^2}s\Delta\bar{p}_f(x,s)\sum_{n=1}^{\infty}\frac{1}{s+\sigma\eta_m n^2}=(\phi c_t)_m s\Delta\bar{p}_m(x,s) \quad [B33]$$

Rearranging gives the pressure drop in the matrix at any location and time in the Laplace domain:

$$\Delta\bar{\hat{p}}_m(x,s)=\frac{(0.006328)k_m}{(\phi c_t)_m\mu}\sigma\frac{6}{\pi^2}\Delta\bar{p}_f(x,s)\sum_{n=1}^{\infty}\frac{1}{s+\sigma\eta_m n^2} \quad [B34]$$

B.2 Laplace Domain Solutions for Non-Uniform Spherical Matrix Blocks

For non-uniform matrix block distribution, such as N_b different spherical matrix blocks, I modify the fracture pressure solution in the Laplace domain. The dual-porosity pressure diffusivity equation for 1-D linear flow for this problem in the Laplace domain is:

$$\left(0.006328\frac{k_{f,eff}}{\mu}\right)\frac{\partial^2\Delta\bar{p}_f(x,s)}{\partial x^2}-f_1\bar{\tau}_1-f_2\bar{\tau}_2=(\phi c_t)_f s\Delta\bar{p}_f(x,s) \quad [B35]$$

And the unsteady-state transfer function for each matrix block in the Laplace domain is:

$$\bar{\tau}_i(x,s)=(0.006328)\frac{k_{m,i}}{\mu}\sigma_i\frac{6}{\pi^2}s\Delta\bar{p}_f(x,s)\sum_{n=1}^{\infty}\frac{1}{s+\sigma_i\eta_{m,i}n^2};\quad i=1,2,...,N_b \quad [B36]$$

Also, the diffusivity constant and shape factor for each type of spherical matrix block are given as followings:

$$\eta_{m,i}=(0.006328)\frac{k_{m,i}}{(\phi\mu c_t)_{m,i}};\quad i=1,2,...,N_b \quad [B37]$$

$$\sigma_i = \frac{\pi^2}{r_{m,i}^2}; \quad i = 1,2,...,N_b \tag{B38}$$

If we follow the same procedure as uniform matrix block solution, the fracture pressure solution for multiple-matrix in the Laplace domain for constant terminal rate case becomes:

$$\Delta\bar{p}_f(x,s) = \frac{1}{s\sqrt{g(s)}} \frac{qB\mu}{(0.006328)k_{f,eff}hL} \exp\left(-\sqrt{g(s)}\,x\right) \tag{B39}$$

Where the new form of *g(s)* is:

$$g(s) = s\begin{bmatrix} \dfrac{(\phi\mu c_t)_f}{(0.006328)k_{f,eff}} + f_1 \dfrac{k_{m,1}}{k_{f,eff}} \sigma_1 \dfrac{6}{\pi^2} \displaystyle\sum_{n=1}^{\infty} \dfrac{1}{s + \sigma_1 \eta_{m,1} n^2} \\ + f_2 \dfrac{k_{m,2}}{k_{f,eff}} \sigma_2 \dfrac{6}{\pi^2} \displaystyle\sum_{n=1}^{\infty} \dfrac{1}{s + \sigma_2 \eta_{m,2} n^2} \\ \vdots \\ + f_{N_b} \dfrac{k_{m,N_b}}{k_{f,eff}} \sigma_{N_b} \dfrac{6}{\pi^2} \displaystyle\sum_{n=1}^{\infty} \dfrac{1}{s + \sigma_{N_b} \eta_{m,N_b} n^2} \end{bmatrix} \tag{B40}$$

The matrix volumetric average pressures in each matrix blocks can also be calculated by using the following equation:

$$\Delta\bar{\hat{p}}_{m,i}(x,s) = \frac{(0.006328)k_{m,i}}{(\phi c_t)_{m,i}\,\mu} \sigma_i \frac{6}{\pi^2} \Delta\bar{p}_f(x,s) \sum_{n=1}^{\infty} \frac{1}{s + \sigma_i \eta_{m,i} n^2}; \quad i = 1,2,...,N_b \tag{B41}$$

APPENDIX C

DERIVATION OF NUMERICAL SOLUTION FOR MULTIPLE-MATRIX PSS MODEL

We will start with the multiple-matrix form of the diffusivity equation, **Eq. 2.4**, and the pseudo-steady state transfer function (**Eq. 4.11** and **Eq. 4.12**) to derive the numerical solution. The 1D diffusivity equation for N_b different matrix blocks is:

$$\frac{\partial}{\partial x}\left(0.006328\frac{k_{f,eff}}{\mu}\right)\frac{\partial p_f(x,t)}{\partial x} - f_1\tau_1 - f_2\tau_2 - \ldots - f_{N_b}\tau_{N_b} + \hat{q} = \left(\phi c_t\right)_f \frac{\partial p_f(x,t)}{\partial t} \qquad [C1]$$

The pseudo-steady state transfer functions for each matrix block in a multiple-matrix model:

$$\tau_j = \left(0.006328\right)\sigma_j \frac{k_{m,j}}{\mu}\left(p_f - p_{m,j}\right); \quad j = 1,2,...,N_b \qquad [C2]$$

And:

$$\left(0.006328\right)\sigma_j \frac{k_{m,j}}{\mu}\left(p_f - p_{m,j}\right) = \left(\phi c_t\right)_{m,j} \frac{\partial p_{m,j}}{\partial t}; \quad j = 1,2,...,N_b \qquad [C3]$$

Combining of **Eq. C1** and **C2** gives:

$$\frac{\partial}{\partial x}\left(0.006328\frac{k_{f,eff}}{\mu}\right)\frac{\partial p_f}{\partial x} - \begin{bmatrix} f_1\left(0.006328\right)\sigma_1 \dfrac{k_{m_1}}{\mu}\left(p_f - p_{m_1}\right) + \\ f_2\left(0.006328\right)\sigma_2 \dfrac{k_{m_2}}{\mu}\left(p_f - p_{m_2}\right) + \\ \vdots \\ f_{N_b}\left(0.006328\right)\sigma_{N_b} \dfrac{k_{m_{N_b}}}{\mu}\left(p_f - p_{m_{N_b}}\right) \end{bmatrix} + \hat{q} = \left(\phi c_t\right)_f \frac{\partial p_f}{\partial t} \qquad [C4]$$

The numerical discretization of above differential equation using the finite difference method is:

$$\frac{1}{\Delta x_i}\left[\left(0.006328\frac{k_{f,eff}}{\mu}\right)_{i+1/2}\frac{p_{f,i+1}^{n+1}-p_{f,i}^{n+1}}{\Delta x_{i+1/2}}-\left(0.006328\frac{k_{f,eff}}{\mu}\right)_{i-1/2}\frac{p_{f,i}^{n+1}-p_{f,i-1}^{n+1}}{\Delta x_{i-1/2}}\right]-$$
$$\left[\begin{array}{l} f_1\left(\left(0.006328\right)\sigma_1\frac{k_{m_1}}{\mu}\right)_i\left(p_{f,i}^{n+1}-p_{m_1,i}^{n+1}\right)+ \\ f_2\left(\left(0.006328\right)\sigma_2\frac{k_{m_2}}{\mu}\right)\left(p_{f,i}^{n+1}-p_{m_2,i}^{n+1}\right)+ \\ \vdots \\ f_{N_b}\left(\left(0.006328\right)\sigma_{N_b}\frac{k_{m_{N_b}}}{\mu}\right)\left(p_{f,i}^{n+1}-p_{m_{N_b},i}^{n+1}\right) \end{array}\right]+\hat{q}_i=\left(\phi c_t\right)_{f,i}^{n}\frac{p_{f,i}^{n+1}-p_{f,i}^{n}}{\Delta t} \qquad \text{[C5]}$$

Multiplying both sides by the volume of each grid block, $\left(V_i=\Delta x_i\Delta y\Delta z\right)$, gives:

$$\left(0.006328\frac{k_{f,eff}}{\mu}\right)_{i+1/2}\frac{\Delta y\Delta z}{\Delta x_{i+1/2}}\left(p_{f,i+1}^{n+1}-p_{f,i}^{n+1}\right)-\left(0.006328\frac{k_{f,eff}}{\mu}\right)_{i-1/2}\frac{\Delta y\Delta z}{\Delta x_{i-1/2}}\left(p_{f,i}^{n+1}-p_{f,i-1}^{n+1}\right)-$$
$$V_i\left[\begin{array}{l} f_1\left(\left(0.006328\right)\sigma_1\frac{k_{m_1}}{\mu}\right)_i\left(p_{f,i}^{n+1}-p_{m_1,i}^{n+1}\right)+ \\ f_2\left(\left(0.006328\right)\sigma_2\frac{k_{m_2}}{\mu}\right)\left(p_{f,i}^{n+1}-p_{m_2,i}^{n+1}\right)+ \\ \vdots \\ f_{N_b}\left(\left(0.006328\right)\sigma_{N_b}\frac{k_{m_{N_b}}}{\mu}\right)\left(p_{f,i}^{n+1}-p_{m_{N_b},i}^{n+1}\right) \end{array}\right]+q_i=\frac{V_i\left(\phi c_t\right)_{f,i}^{n}}{\Delta t}\left(p_{f,i}^{n+1}-p_{f,i}^{n}\right) \qquad \text{[C6]}$$

The matrix-fracture transfer function equations, **Eq. C3**, for node *i* (Here *i* denotes the node number and *j* denotes the matrix block number) for N_b different matrix block can be written as:

$$\left(\left(0.006328\right)\sigma_j\frac{k_{m_j}}{\mu}\right)_i\left(p_{f,i}^{n+1}-p_{m_j,i}^{n+1}\right)=\left(\phi c_t\right)_{m_j,i}\frac{p_{m_j,i}^{n+1}-p_{m_j,i}^{n}}{\Delta t};\quad j=1,2,...,N_b \qquad \text{[C7]}$$

Solving the transfer function equation for matrix pressure, $p_{m_j,i}^{n+1}$, gives:

$$p_{m_j,i}^{n+1}=\left(\frac{\frac{\left(\phi c_t\right)_{m_j,i}^{n}}{\Delta t}}{\left[\left(0.006328\right)\sigma_j\frac{k_{m_j}}{\mu}\right]_i+\frac{\left(\phi c_t\right)_{m_j,i}^{n}}{\Delta t}}\right)p_{m_j,i}^{n}+\left(\frac{\left[\left(0.006328\right)\sigma_j\frac{k_{m_j}}{\mu}\right]_i}{\left[\left(0.006328\right)\sigma_j\frac{k_{m_j}}{\mu}\right]_i+\frac{\left(\phi c_t\right)_{m_j,i}^{n}}{\Delta t}}\right)p_{f,i}^{n+1} \qquad \text{[C8]}$$

And substituting into the diffusivity equation yields:

$$\left(0.006328\frac{k_{f,eff}}{\mu}\right)_{i+\frac{1}{2}}\frac{\Delta y\Delta z}{\Delta x_{i+\frac{1}{2}}}\left(p_{f,i+1}^{n+1}-p_{f,i}^{n+1}\right)-\left(0.006328\frac{k_{f,eff}}{\mu}\right)_{i-\frac{1}{2}}\frac{\Delta y\Delta z}{\Delta x_{i-\frac{1}{2}}}\left(p_{f,i}^{n+1}-p_{f,i-1}^{n+1}\right)-$$

$$V_i\left[\begin{array}{l}
f_1\left((0.006328)\sigma_1\frac{k_{m_1}}{\mu}\right)_i\left(\begin{array}{l}p_{f,i}^{n+1}-\left(\frac{\frac{(\phi c_t)_{m_1,i}^n}{\Delta t}}{\left[(0.006328)\sigma_1\frac{k_{m_1}}{\mu}\right]_i+\frac{(\phi c_t)_{m_1,i}^n}{\Delta t}}\right)p_{m_1,i}^n\\ -\left(\frac{\left[(0.006328)\sigma_1\frac{k_{m_1}}{\mu}\right]_i}{\left[(0.006328)\sigma_1\frac{k_{m_1}}{\mu}\right]_i+\frac{(\phi c_t)_{m_1,i}^n}{\Delta t}}\right)p_{f,i}^{n+1}\end{array}\right)+\\
f_2\left((0.006328)\sigma_2\frac{k_{m_2}}{\mu}\right)\left(\begin{array}{l}p_{f,i}^{n+1}-\left(\frac{\frac{(\phi c_t)_{m_2,i}^n}{\Delta t}}{\left[(0.006328)\sigma_2\frac{k_{m_2}}{\mu}\right]_i+\frac{(\phi c_t)_{m_2,i}^n}{\Delta t}}\right)p_{m_2,i}^n\\ -\left(\frac{\left[(0.006328)\sigma_2\frac{k_{m_2}}{\mu}\right]_i}{\left[(0.006328)\sigma_2\frac{k_{m_2}}{\mu}\right]_i+\frac{(\phi c_t)_{m_2,i}^n}{\Delta t}}\right)p_{f,i}^{n+1}\end{array}\right)+\\
\vdots\\
f_{N_b}\left((0.006328)\sigma_{N_b}\frac{k_{m_{N_b}}}{\mu}\right)\left(\begin{array}{l}p_{f,i}^{n+1}-\left(\frac{\frac{(\phi c_t)_{m_{N_b},i}^n}{\Delta t}}{\left[(0.006328)\sigma_{N_b}\frac{k_{m_{N_b}}}{\mu}\right]_i+\frac{(\phi c_t)_{m_{N_b},i}^n}{\Delta t}}\right)p_{m_{N_b},i}^n\\ -\left(\frac{\left[(0.006328)\sigma_{N_b}\frac{k_{m_{N_b}}}{\mu}\right]_i}{\left[(0.006328)\sigma_{N_b}\frac{k_{m_{N_b}}}{\mu}\right]_i+\frac{(\phi c_t)_{m_{N_b},i}^n}{\Delta t}}\right)p_{f,i}^{n+1}\end{array}\right)
\end{array}\right] \qquad [C9]$$

$$q_{f,i}=\frac{V_i(\phi c_t)_{f,i}^n}{\Delta t}\left(p_{f,i}^{n+1}-p_{f,i}^n\right)$$

Or:

$$\left(0.006328\frac{k_{f,eff}}{\mu}\right)_{i+\frac{1}{2}}\frac{\Delta y\Delta z}{\Delta x_{i+\frac{1}{2}}}\left(p_{f,i+1}^{n+1}-p_{f,i}^{n+1}\right)-\left(0.006328\frac{k_{f,eff}}{\mu}\right)_{i-\frac{1}{2}}\frac{\Delta y\Delta z}{\Delta x_{i-\frac{1}{2}}}\left(p_{f,i}^{n+1}-p_{f,i-1}^{n+1}\right)-$$

$$V_i\left[\sum_{j=1}^{N_b}f_j\left(\left(0.006328\right)\sigma_j\frac{k_{m_j}}{\mu}\right)_i\left(\begin{array}{l}p_{f,i}^{n+1}-\left(\dfrac{\dfrac{\left(\phi c_t\right)_{m_j,i}^{n}}{\Delta t}}{\left[\left(0.006328\right)\sigma_j\dfrac{k_{m_j}}{\mu}\right]_i+\dfrac{\left(\phi c_t\right)_{m_j,i}^{n}}{\Delta t}}\right)p_{m_j,i}^{n}\\-\left(\dfrac{\left[\left(0.006328\right)\sigma_j\dfrac{k_{m_j}}{\mu}\right]_i}{\left[\left(0.006328\right)\sigma_j\dfrac{k_{m_j}}{\mu}\right]_i+\dfrac{\left(\phi c_t\right)_{m_j,i}^{n}}{\Delta t}}\right)p_{f,i}^{n+1}\end{array}\right)\right] \qquad [C10]$$

$$q_{f,i}=\frac{V_i\left(\phi c_t\right)_{f,i}^{n}}{\Delta t}\left(p_{f,i}^{n+1}-p_{f,i}^{n}\right)$$

After rearranging, we obtain:

$$p_{f,i-1}^{n+1}\left[\left(\frac{0.006328k_{f,eff}}{\mu}\right)_{i-\frac{1}{2}}\frac{\Delta y\Delta z}{\Delta x_{i-\frac{1}{2}}}\right]+p_{f,i+1}^{n+1}\left[\left(\frac{0.006328k_{f,eff}}{\mu}\right)_{i+\frac{1}{2}}\frac{\Delta y\Delta z}{\Delta x_{i+\frac{1}{2}}}\right]+$$

$$p_{f,i}^{n+1}\left[\begin{array}{l}-\left(\dfrac{0.006328k_{f,eff}}{\mu}\right)_{i-\frac{1}{2}}\dfrac{\Delta y\Delta z}{\Delta x_{i-\frac{1}{2}}}-\left(\dfrac{0.006328k_{f,eff}}{\mu}\right)_{i+\frac{1}{2}}\dfrac{\Delta y\Delta z}{\Delta x_{i+\frac{1}{2}}}\\-\dfrac{V_i\left(\phi c_t\right)_{f,i}^{n}}{\Delta t}-V_i\displaystyle\sum_{j=1}^{N_b}\left(f_j\left(\left(0.006328\right)\sigma_j\dfrac{k_{m_j}}{\mu}\right)_i-\dfrac{f_j\left(\left(0.006328\right)^2\sigma_j^2\dfrac{k_{m_j}^2}{\mu^2}\right)_i}{\left(\left(0.006328\right)\sigma_j\dfrac{k_{m_j}}{\mu}\right)_i+\dfrac{\left(\phi c_t\right)_{m_j,i}^{n}}{\Delta t}}\right)\end{array}\right]$$

$$=-\frac{V_i\left(\phi c_t\right)_{f,i}^{n}}{\Delta t}p_{f,i}^{n}-q_i-V_i\sum_{j=1}^{N_b}\left(\frac{f_j\left(\left(0.006328\right)\sigma_j\dfrac{k_{m_j}}{\mu}\right)_i\dfrac{\left(\phi c_t\right)_{m_j,i}^{n}}{\Delta t}}{\left(\left(0.006328\right)\sigma_j\dfrac{k_{m_j}}{\mu}\right)_i+\dfrac{\left(\phi c_t\right)_{m_j,i}^{n}}{\Delta t}}\right)p_{m_j,i}^{n} \qquad [C11]$$

We define the coefficient of the three-banded solution matrix and the right hand side vector as following:

$$D_i p_{f,i-1}^{n+1} + E_i p_{f,i}^{n+1} + F_i p_{f,i+1}^{n+1} = R_i \qquad \text{[C12]}$$

Where:

$$D_i = \left(\frac{0.006328 k_{f,eff}}{\mu} \right)_{i-1/2} \frac{\Delta y \Delta z}{\Delta x_{i-1/2}} \qquad \text{[C13]}$$

$$F_i = \left(\frac{0.006328 k_{f,eff}}{\mu} \right)_{i+1/2} \frac{\Delta y \Delta z}{\Delta x_{i+1/2}} \qquad \text{[C14]}$$

$$E_i = -\left[D_i + F_i + \frac{V_i \left(\phi c_t\right)_{f,i}^{n}}{\Delta t} + V_i \sum_{j=1}^{N_b} \left(\frac{f_j \left(\left(0.006328\right) \sigma_j \frac{k_{m_j}}{\mu} \right)_i - f_j \left(\left(0.006328\right)^2 \sigma_j^2 \frac{k_{m_j}^2}{\mu^2} \right)_i}{\left(\left(0.006328\right) \sigma_j \frac{k_{m_j}}{\mu} \right)_i + \frac{\left(\phi c_t\right)_{m_j,i}^{n}}{\Delta t}} \right) \right] \qquad \text{[C15]}$$

$$R_i = -\frac{V_i \left(\phi c_t\right)_{f,i}^{n}}{\Delta t} p_{f,i}^{n} - q_i - V_i \sum_{j=1}^{N_b} \left(\frac{f_j \left(\left(0.006328\right) \sigma_j \frac{k_{m_j}}{\mu} \right)_i \frac{\left(\phi c_t\right)_{m_j,i}^{n}}{\Delta t}}{\left(\left(0.006328\right) \sigma_j \frac{k_{m_j}}{\mu} \right)_i + \frac{\left(\phi c_t\right)_{m_j,i}^{n}}{\Delta t}} \right) p_{m_j,i}^{n} \qquad \text{[C16]}$$